Journal of Applied Physics

PERSPECTIVE | FEBRUARY 24 2026

Light-induced damage in semiconductor device manufacturing: Present and future challenges

Ester Abram; Reynolds Dziobek-Garrett; Vina Faramarzi; Roland Bliem; Paul Planken

J. Appl. Phys. 139, 080901 (2026)
https://doi.org/10.1063/5.0308054

Articles You May Be Interested In

Sub-ablation-threshold light-induced modification of thin ruthenium layers detected using optical reflectance

J. Appl. Phys. (December 2024)

Enhanced second-harmonic generation from $WS_2/ReSe_2$ heterostructure

J. Chem. Phys. (March 2026)

Advancing microelectronics through nanoscale science: A perspective on needs and opportunities from the nanoscale science research centers

Appl. Phys. Rev. (October 2025)

26 March 2026 13:26:42

Journal of Applied Physics PERSPECTIVE pubs.aip.org/aip/jap

Light-induced damage in semiconductor device manufacturing: Present and future challenges

Cite as: J. Appl. Phys. **139**, 080901 (2026); doi: 10.1063/5.0308054
Submitted: 20 October 2025 · Accepted: 12 January 2026 ·
Published Online: 24 February 2026

View Online

Export Citation

CrossMark

Ester Abram,[1,2,3,a)] Reynolds Dziobek-Garrett,[1,2] Vina Faramarzi,[4] Roland Bliem,[1,2] and Paul Planken[1,2]

AFFILIATIONS

[1]Advanced Research Center for Nanolithography (ARCNL), Science Park 106, 1098 XG Amsterdam, The Netherlands
[2]Van der Waals-Zeeman Institute, Institute of Physics, University of Amsterdam, Science Park 904, 1098 XH Amsterdam, The Netherlands
[3]LaserLaB, Physics & Astronomy Department, Vrije Universiteit Amsterdam, De Boelelaan 1100, 1081 HZ Amsterdam, The Netherlands
[4]ASML Netherlands B.V., De Run 6501, 5504 DR Veldhoven, The Netherlands

[a)]**Author to whom correspondence should be addressed:** e.abram@vu.nl

26 March 2026 13:26:42

ABSTRACT

Advances in semiconductor manufacturing over the past few decades, driven by the need for smaller, faster, and more efficient devices, have pushed enormous progress in light sources for lithography and metrology. However, the smaller feature sizes and more costly wafer real estate necessitate smaller spot sizes, smaller test/alignment markers, and higher light intensities. This combination has made light-induced damage an obstacle to fast, reliable wafer-lithography, -metrology, -leveling, and -alignment. In this perspective, we address the challenges of light-induced damage for semiconductor manufacturing, highlighting the light sources, materials, device stacks, and damage mechanisms at play. Furthermore, we provide a perspective into the future of the industry and of new materials, which provide new functionality, but may be more sensitive to light-induced damage. Finally, we discuss how light-induced damage can be used constructively, for instance, in direct laser writing or material processing.

© 2026 Author(s). All article content, except where otherwise noted, is licensed under a Creative Commons Attribution (CC BY) license (https://creativecommons.org/licenses/by/4.0/). https://doi.org/10.1063/5.0308054

I. INTRODUCTION

Light-induced damage (LID) has been studied extensively in the past, particularly since the invention of the Q-switched laser in the late 1950s and early 1960s,[1,2] which enabled laser pulse durations of tens of nanoseconds. Although high-quality optical components were available, even small surface defects that passed quality control could trigger LID when exposed to these powerful lasers. With these high powers, the field of nonlinear optics took off, giving rise to new mechanisms for LID, such as self-focusing.[3] Now, tightly focused, relatively modest-energy laser pulses can generate electric fields strong enough to induce dielectric breakdown in materials used for laser components[4] (pp. 3–4). For much of the LID research, largely focused on optical components,[4] a more phenomenological approach is often taken to examine how various factors influence LID thresholds, such as used material,[5] wavelength,[6–8] pulse duration,[9–11] repetition rate,[12] (p. 6) and film thickness.[13,14] In this perspective, we shift the focus toward the materials and light sources relevant to the semiconductor manufacturing industry, aiming to understand the underlying physical processes of LID in this context.

To minimize the risk of LID, the light intensity can be reduced by lowering the pulse energy, increasing the spot size, or extending the pulse duration if the damage is nonthermal in origin. While these measures may be feasible for optical components in laser systems, the semiconductor manufacturing industry often requires high fluences, for instance, in nanolithographic processes and wafer alignment measurements. In semiconductor manufacturing, integrated circuits (ICs) are fabricated, which consist of hundreds of layers containing complex patterns.[15] Nowadays, the most complex and miniaturized ICs are fabricated with the use of

© Author(s) 2026

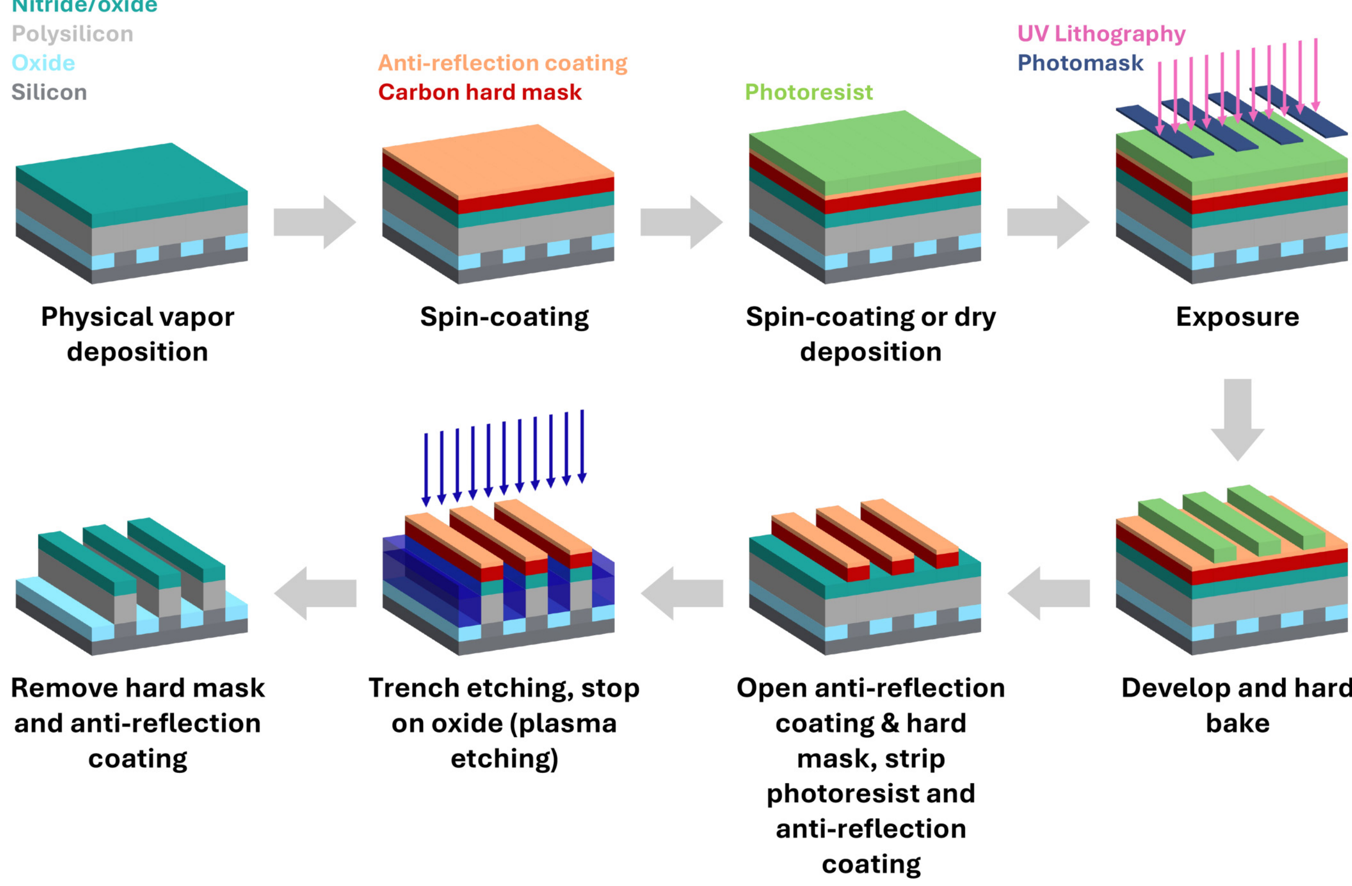

FIG. 1. Sequential steps in fabricating a typical semiconductor device layer, from material deposition and photoresist coating to UV-based lithography exposure, development, and plasma etching, illustrating the layered structure and process flow including different materials for pattern transfer and final trench formation. Prior to the lithography step, the film thickness, uniformity, and defectivity will be controlled. Leveling and alignment are performed during the lithography step. Postlithography metrology and inspection steps are defect inspection, CD and overlay measurements, etch depth and profiling, etc. (see Sec. II A).

26 March 2026 13:26:42

extreme ultraviolet (EUV) photolithography, using complex EUV ‘scanners’, which use reflective optics to print patterns into photoresists with nanoscale features. In addition to the possibility of LID from exposure of various components and materials to EUV light, even the process of EUV generation presents a substantial risk; this is done through the generation of Sn plasma, which requires IR pump fluences in the kW regime for sufficient EUV light. Once the pattern has been printed into the photoresist, a combination of etching, deposition, and other processing steps is used to create the desired layer within the device stack, as is schematically shown in Fig. 1. These layers and patterns are increasingly at risk of optical damage[16,17] due to the increasingly high light fluence required for precise wafer positioning and inspection.[18,19] Alignment markers, often in the form of small gratings, are etched into the scribe lanes between the dies on the wafer; light diffracted by these markers is used to measure the wafer position.[20] To save wafer real estate, these alignment gratings are becoming smaller,[21,22] which forces a concomitant decrease in the illuminated area. To keep the same amount of diffracted light, and thus the same signal-to-noise-ratio, an increase in incident optical fluence is required. Both the increasing light intensity and the decreasing size of the nanostructures etched into these layers amplify the risk of LID through localized field enhancements.[23] Once a layer or pattern has been printed, it is also necessary to inspect it for imperfections. These *metrology* steps are also often carried out with light-based techniques, and various competing requirements similarly increase the potential for LID to IC components during these steps. In addition to current risks, future innovations may also face significant challenges related to LID. For example, the integration of novel materials, such as two-dimensional (2D) materials in future devices, could be critically hindered by their susceptibility to light-induced damage. It is, therefore, critical to properly assess LID for each of these materials within the realm of semiconductor manufacturing. For example, metrology markers should be designed by co-optimizing material properties, such as refractive index and absorption, taking the light-induced damage threshold (LIDT) of these materials into account.

© Author(s) 2026

But what exactly is light-induced damage? While it is often associated with fully destructive effects, such as those seen in laser cutting,[24,25] LID can also cause more subtle, localized material modifications.[26,27] In some cases, these changes are beneficial and can even be useful for advanced applications, for instance, the direct writing of patterns below the diffraction limit[28,29] without using a photoresist.

Light-induced damage poses numerous risks throughout the entire nanolithography fabrication process, both in current technologies and in future developments. In this perspective paper, we aim to address, describe, and discuss these challenges. We, therefore, focus on a targeted subset of LID challenges specific to lithographic processes and wafer metrology, for example, during wafer alignment. Accordingly, we provide an overview of current and future light sources relevant to these issues, as well as the corresponding wafer materials and optical components that are, or will be, exposed by those light sources. In Sec. II, we provide an overview of the key bottlenecks that we believe are critical to understanding LID risks. This collection of insights has emerged from collaborations with a broad community of scientists and engineers engaged in nanolithography research and development. In Sec. III, we highlight emerging materials and light sources, and we introduce methods for utilizing controlled LID effects for nanofabrication or (general) inspection. Through this, we aim to present the reader with a comprehensive view of the challenges and opportunities associated with LID in the semiconductor manufacturing industry. We expect research into LID to remain fruitful over the coming years, especially at the interface of fundamental physics research and the semiconductor industry.

II. CURRENT RESEARCH

The onset of optical damage is not solely determined by some critical value of the total energy or the peak fluence of the light. Peak fluence, pulse duration, repetition rate, and wavelength/bandwidth can also play significant roles. In addition to these *light parameters*, the characteristics of the layer and the material it is made of also influence the onset of damage. *Layer parameters*, such as thickness, material, refractive index, surface topography, stack composition, and adhesion to surrounding layers, all contribute to where the light is absorbed and how and where the material is affected. The total parameter space that determines the light-induced damage threshold is, therefore, huge. To provide a focused and practical framework for investigation, we introduce a selected subset of parameters that are most relevant to our study and will be explored in greater detail in this section.

A. Patterning, metrology, and inspection in semiconductor manufacturing

Metrology and inspection play a critical role in semiconductor manufacturing by monitoring and controlling the quality and conformity of the structures and materials that form semiconductor devices through various layers and processing sequences. The primary goal of this is to reduce costs by maximizing yield and accelerating time to market. While general wafer inspection detects surface particles, pattern flaws, and other conditions that could affect the performance of the finished device, metrological procedures ensure that the *physical* and *electrical* properties of the devices being produced are met at each stage.

A combination of inline and offline metrology and inspection techniques support semiconductor manufacturing. Inline metrology refers to measurement techniques that are integrated directly into the production line, allowing for real-time or near-real-time monitoring of wafers without removing them from the process flow. This enables rapid feedback and process control, minimizing defects and improving yield. In contrast, offline metrology involves taking wafers out of the production line for more detailed or specialized analysis in a separate lab environment. While offline methods often provide higher precision and a broader range of measurements, they are slower, often invasive, and less suited for immediate process adjustments. Both approaches are complementary, balancing speed and accuracy in quality control. Table I summarizes an overview of metrology and inspection systems, and Fig. 2 shows the typical wavelengths used by them.

As listed in Table I, various sources are employed in metrology and inspection systems to cover different materials and stacks, penetration depths, and measurement parameters. These include photons across the visible, near-infrared, and ultraviolet (UV) spectral ranges, as well as electrons with tunable landing energies and acceleration voltages. Lasers are also being integrated in electron beam systems to mitigate charging effects, especially in materials, such as EUV resists or low-κ[30] dielectrics with low conductivity.

There is currently a rich research landscape for metrology techniques, which encompass the ever-expanding world of semiconductor fabrication. This includes using broadband light sources for more optimized alignment recipes, where a broad wavelength range between 200 and 1300 nm is more robust to changes in the material and structure.[31] The metrology targets for overlay, alignment, and leveling themselves are also the subject of new research. Dedicated structures, called *test markers* or *targets*, are included in the photolithography masks, called *reticles* in extreme ultraviolet (EUV) systems, and are printed on the wafers along with the desired device patterns. These structures are typically placed in the scribe lane between dies, or even within the die itself to correct for die differences. These occupy valuable wafer real estate, and thus, reducing their size is crucial. Furthermore, optimized test marker designs to increase sensitivity and specificity are also being explored. Such marker designs need to take into account not only the desired light coupling and size requirements, but also the materials from which they are composed. Often, the test markers are composed of photoresists themselves, and decreasing resist thickness and novel compositions as in EUV lithography must also be taken into account. Figure 3 shows two “diffraction based overlay metrology stacks,” which are used as alignment markers. Finally, the increasing number of processing steps (see Fig. 1), including the bonding of wafers and dies for 3D integration and advanced packaging, put significantly more stress on a wafer, causing in some cases severe and complex deformations. For overlay and alignment, these need to be rigorously measured, requiring significantly more measurements to accurately account for them. Faster measurement techniques are, thus, highly sought after, with innovations, including multi-laser and

26 March 2026 13:26:42

© Author(s) 2026

TABLE I. Overview of metrology and inspection systems.

	Tool type	Purpose	Source	Features
Optical	Ellipsometry	Measures film thickness and optical properties	UV to NIR (200–1000 nm)	Uses polarized light; sensitive when using thin films
	Spectroscopic reflectometry	Measures film thickness and refractive index	Broadband white light (UV-VIS-NIR)	Non-destructive, fast
	Scatterometry	Measures critical dimension (CD), overlay, and side-wall angle	Can be DUV-UV-VIS and extended to some NIR ($\approx 1\,\mu$m) with broadband white light	Indirect method using diffraction patterns, fast
	Optical critical dimension (OCD) metrology, scattering, and inspection	CD, thickness, profile, and pattern defect inspection	DUV (193 nm), visible light	DUV provides enhanced resolution, contrast, and sensitivity
Electron and x ray	Critical dimension SEM (CD-SEM)	Measures critical dimensions of features (line widths, contact hole diameter, spaces, and pitches)	Electron beam (not light)	High resolution and critical for process control. Low throughput with charging effects
	E-beam overlay metrology	Pattern placement and overlay measurement	Electron beam	Critical for EUV layers, Slow and complex (large amount of data)
	E-beam inspection	Defect detection (yield monitoring)	Electron beam	High sensitivity to small defects, slow scan speed, and expensive
	Voltage contrast SEM	Identified electrical defects (e.g., opens/shorts)	Electron beam	Non-destructive, reveals electrical anomalies. Limited to conductive paths
	(Scanning) transmission electron microscopy (STEM)	Atomic-level imaging and analysis	Electron beam	Extremely high resolution, elemental analysis, complex sample preparation
	X-ray reflectometry (XRR)	Film thickness, density, roughness	X-ray tube (Cu Kα, etc.)	Non-destructive, high precision, complex modeling
	X-ray diffraction (XRD)	Crystal structure, strain	X-ray tube (Cu Kα, etc.)	Used for epitaxial layers
	Critical dimension small angle x-ray scattering (CD-SAXS)	3D CD metrology, increasingly used for advanced modes, e.g., GAA or FinFET	High precision for high aspect ratio features	Complex modeling
Infrared and Raman spectroscopy	Fourier transform infrared (FTIR)	Film thickness, composition, bonding	IR source (Globar, etc.)	Fast, non-destructive, limited spatial resolution, surface sensitive
	Raman spectroscopy	Stress, strain, crystallinity	Laser (532, 785 nm, etc.)	High spatial resolution, slow mapping
Atomic and scanning probe	Atomic force microscopy (AFM)	Surface topography, roughness, CD	Laser (for cantilever detection)	High resolution, 3D profiling, slow
	Other scanning probe microscopy (SPM)	Electrical, magnetic, and mechanical properties	Laser (for feedback)	Mostly R&D, for failure analysis and materials development

burst-mode operation. While the research into the metrology parameter space is enormous, the bottom line is that a larger number of faster measurements on smaller test markers leads to significantly more risk of LID.

B. Light sources for next generation metrology

Next-generation metrology equipment is needed to enable high-yield high-volume manufacturing of advanced semiconductor nodes (5 nm, 3 nm, and beyond[31]). These systems require light

26 March 2026 13:26:42

© Author(s) 2026

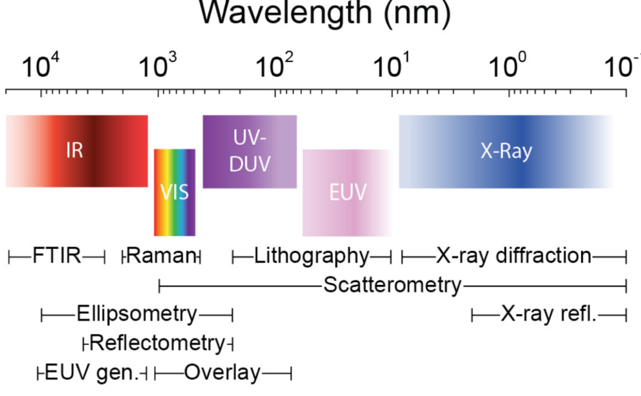

FIG. 2. The electromagnetic spectrum with wavelength ranges and applications relevant to semiconductor manufacturing and metrology. The shown wavelength ranges for each application are also listed in Table S1 of the supplementary material.

sources with exceptional brightness, spectral stability, and coherence to achieve the subnanometer resolution and sensitivity in measuring critical parameters that are essential for accurate and reliable fabrication of high quality device structures.[18,19,33] Such light sources are not widely available as commercial products and often need to be custom developed, potentially tailored for each specific system. Table II lists the key (future) light-source features and their benefits for semiconductor metrology tools, and in Fig. 4, we show the various applications for these light sources and their requirements.

Each metrology system is composed of a moving stage, a source and a sensor. To stay in the safe operating zone, a good estimation of the *power and intensity levels* (i.e., pulse duration, illumination area, absorption depth, and energy per pulse) at each stage of the system from the source exit to the wafer is essential; this is achieved by comparing power and fluence levels to laser-induced damage thresholds of material used in the optical pathway and in the stack on the wafer (see Figs. 1 and 3). Here, the *material present on the wafers* can be composed of different types of amorphous carbon layers, photoresists (e.g., for EUV and DUV), spin-on glass (SOG), spin-on carbon (SOC); insulators, such as SiO_2 and Si_3N_4; semiconductors, such as silicon; metals, such as

TABLE II. Light-source features and benefits in semiconductor metrology.

Feature	Benefit for metrology
Ultra-broadband	Multi-layer, multi-material inspection
High-brightness	Fast, high-resolution measurements
Spatial coherence	Precise alignment and focusing
Spectral tunability	Customizable for specific metrology tasks
Fiber delivery	Easy hardware integration

TiN, tungsten, copper, and ruthenium, etc. Furthermore, *structures and geometries are present*, such as patterns (gratings, contact holes, and 2D patterns), with typical dimensions of the order of the critical dimension (CD), pitch, layer thickness, and feature heights. Not only the material on the wafer, but also the *material in the optical path*, such as the multilayer coating on mirrors and lenses, optical filters, and fibers are exposed to the light.

For ultra-short (fs–ps) pulsed light sources where each pulse can carry microjoules of energy, damage can occur after a single pulse[4] (pp. 165–167). Thus, J/cm^2, or fluence, is a more suitable *unit for determining LID thresholds* of pulsed sources, whereas W/cm^2 is the unit commonly used for the power density of continuous wave (CW) sources where average power is the key determining parameter for energy density transferred to the material, and for ultrashort laser pulses, where peak intensity is relevant to determine the risk of multiphoton excitation. At very high repetition rates (>5 MHz), the time between two pulses might be shorter than the time scales of energy removal from the illuminated volume by carrier transport or heat diffusion. In that case, energy accumulation might lead to damage. The repetition rate where this occurs will depend on heat conductivity and heat capacity and is, thus, material dependent. It is necessary to define the window of parameters for such a transition (e.g., inter-pulse separation time, energy per pulse, and pulse duration). For the development of any new metrology light source, it is necessary to take all these factors into account to avoid damage to the setup or target.

Among new light sources in development for semiconductor manufacturing, supercontinuum white light sources with high photon flux that are broadband, spatially coherent, and highly stable are emerging as promising candidates to address the limitations of traditional broadband sources in resolution and sensitivity. The supercontinuum white light generated through nonlinear processes in photonic crystal fibers or in other nonlinear media offers

26 March 2026 13:26:42

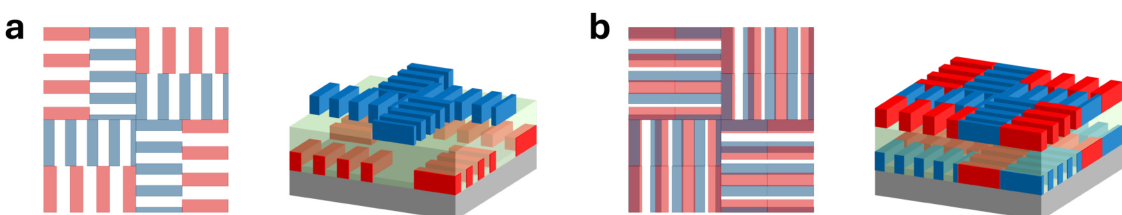

FIG. 3. Two different diffraction based overlay metrology stack structures: (a) an AIM® and (b) a rAIM™ target.[32]

© Author(s) 2026

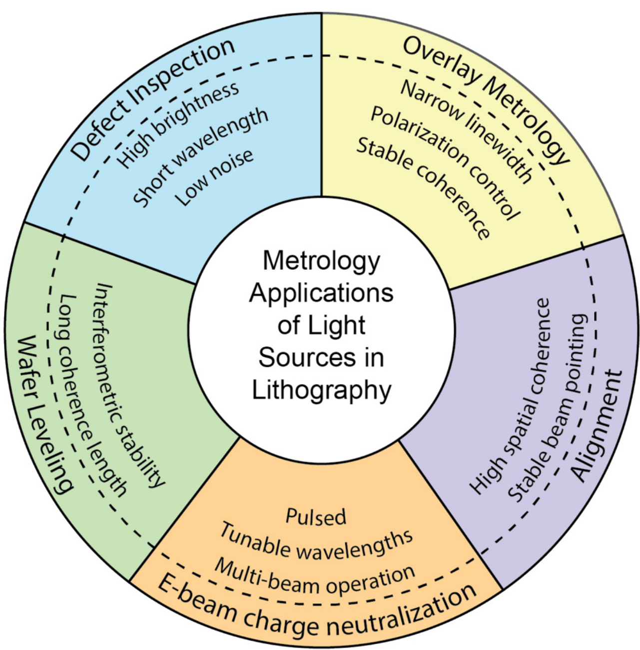

FIG. 4. Schematic representation of light source applications and requirements for metrology.

a continuous spectral range from the visible to near-infrared or even mid-infrared regions and enables multi-wavelength and spectroscopic approaches within a single platform. As metrology tolerances tighten with continued scaling, the tunability and broadband nature of supercontinuum light make it a flexible and powerful tool for future-proof metrology systems in advanced semiconductor manufacturing.

There are several technical and practical challenges on the way of integrating an optical high volume manufacturing (HVM) metrology system[34,35] with a supercontinuum white light source, among which reliability, cost, and compatibility with the fabrication environment are of high value. A combination of very high photon flux and tight focus requirements exposes the fibers, the optical elements in the sensor, and the structures on the wafer to significantly higher local power densities in a very short time (pulse durations of 10^{-14} to 10^{-10} s). This increases the risk of material damage,[26,27] pattern deformation,[23] and eventually product yield loss due to light–matter interaction, and needs to be avoided at all costs.

Light-induced damage can be a critical issue both in the generation and application of broadband high power pulsed light sources in advanced semiconductor metrology. The material damage and degradation can be caused by depositing high peak-power femtosecond or picosecond pulses, via prolonged exposure to high intensities (high average power), or by cumulative thermal effects. For a supercontinuum white-light source, the incident fluence or peak intensity can trigger different damage mechanisms in both the light source and the illuminated material. During the generation of the white-light, the photonic crystal fiber itself may be damaged due to self-focusing, material degradation, or damage to the end-facet. In addition, damage can occur downstream on optical components, such as anti-reflection coatings, mirrors, color filters, and beam splitters in the optical path that are not optimized or tested for such bandwidths and intensities. Moreover, damage can occur on the wafer itself due to the high power, the large bandwidth, and the variety of materials and structures on the wafer, increasing the absorption probability even for single wavelength measurements.

The advancement of supercontinuum sources serves as a microcosm for the development of other new light sources. While supercontinuum sources offer unique advantages for metrology, careful engineering is required to prevent light-induced damage at both the source and application ends. These constraints are especially important as critical dimensions shrink and materials become increasingly delicate. Therefore, we summarize the novel requirements and parameters that need to be considered for a *pulsed (supercontinuum)* light source.

Light absorption of different materials is key information (see Sec. II in the supplementary material). The way a material absorbs light significantly influences how it responds to irradiation. Materials with high absorbance at the laser's wavelength tend to experience rapid energy deposition, leading to localized heating, melting, ablation, or even plasma formation. The bandgap, optical constants, and electronic structure of the material determine its absorbance profile, making wavelength selection crucial for precise material processing. For example, semiconductors, such as silicon, absorb strongly in the visible and near-infrared, while dielectrics may require shorter wavelengths (e.g., UV) for effective interaction. Understanding these absorbance characteristics is essential for understanding light-induced damage mechanisms.

Even in materials that are transparent at the laser wavelength, intense (ultrashort) pulses can deposit energy through nonlinear absorption. The pulses create free carriers by strong-field ionization (SFI),[36,37] which is commonly modeled with Keldysh theory,[38] together with avalanche (impact) ionization.[39,40] Depending on wavelength, field strength, and bandgap, SFI proceeds via a combination of multiphoton ionization (MPI) and tunneling ionization (TI)[4] (pp. 84–116). High field strengths are necessary for strong nonlinear absorption, but direct (linear) absorption in absorbing layers occurs at all fluences. Thus, in stacks with both absorbing and transparent materials, linear absorption in the absorbing layers is typically the limiting factor.

To translate the direct light absorption into damage mechanisms and fluence thresholds, a strong understanding of the physical processes leading to damage, computational models and databases are needed to make *predictions*.[23] Furthermore, we have to incorporate ways to *detect* reaching damage thresholds in materials in future metrology tools (see Sec. IV A).

C. Direct damage by light

1. From light absorption to heat

When light is absorbed, direct damage occurs when the incident fluence exceeds a certain threshold, commonly denoted as the damage threshold fluence F_{th}, measured in J/cm^2. When a

26 March 2026 13:26:42

© Author(s) 2026

material is exposed to light with a fluence above F_{th}, the heat that is generated by the absorption of the light into the material will reach a critical value. This (fast) heating can induce, for instance, a shock wave,[41] and/or induce mechanical stresses,[26,42] melting and evaporation,[43,44] ultimately resulting in catastrophic damage.[9,45,46] To understand how materials can get directly damaged by light, one has to consider the light–matter interaction that takes place. First, the amount and location of absorption in a material or stack of materials must be calculated. This can be done by analytically or numerically solving the Maxwell equations. However, for multilayer stacks, this can be achieved more efficiently using the transfer-matrix method (TMM),[46–48] while for periodic structures, such as gratings, the rigorous coupled-wave analysis (RCWA)[49] may be used to solve the Maxwell equations. However, this assumes that the absorption is linear. In other words, this implies that additional absorption from excited matter, or less absorption from, for instance, shadowing effects, do not occur during excitation.[50–53] For strong laser excitation, this calculated absorption should be modified, e.g., by including these effects. Examples of this can be found in Refs. 16, 17, 50, and 54 for silicon.

The measured or calculated absorbed power density can serve as the initial condition for simulations of the spatial lattice temperature profile shortly after illumination. For metals, the dynamics of the absorbed energy transfer is often described by the two-temperature model (TTM).[55–57] As the term suggests, the two-temperature model assumes that both the electronic and lattice subsystems can be described by their own temperature, and that they can exchange energy via electron–phonon coupling. For time scales longer than the electron thermalization time, the TTM often provides a proper description of the spatial and temporal evolution of the electron gas temperature T_e and the lattice temperature T_l, although the model is not particularly good for certain metals, such as ruthenium.[58]

A few picoseconds after optical excitation (depending on the material and stack geometry), the electron and lattice temperatures in the absorbing metal are in equilibrium, as calculated by the two-temperature model (TTM). From this point onward, the system's overall (lattice) temperature T can be determined by solving the single-temperature heat diffusion equation[59,60] (Sec. II C in the supplementary material). This model helps to understand laser damage phenomenologically. In the following, we discuss various regimes where it is applicable.

2. Single-shot damage (1-on-1)

As previously noted, metrology applications require materials to be exposed to the highest possible light fluence without surpassing the damage threshold. To achieve this, a key advancement involves transitioning from continuous-wave (CW) light sources to femtosecond or picosecond pulsed lasers (see Sec. II B). This shift enables the wafer to be irradiated with a series of high-intensity pulses with enough time between pulses to allow cooling of the material. Due to the rapid heating induced by these (ultra)fast laser pulses, and the subsequent cooling, a variety of damage processes can occur. These include surface cracking,[27] top-level ablation,[16,27] grain structure change,[26] and other surface morphology changes.[27,61] To develop a thorough understanding of these complex processes, it is crucial to begin with the simplest case—single-shot damage measurements [1-on-1[4] (pp. 165–167),[62] (p. 8)]. These experiments isolate the effects of an individual laser pulse, avoiding the confounding influence of cumulative damage from multiple exposures. In LID research, single-shot measurements are a standard initial step, especially when the underlying damage mechanisms are not yet well understood. Once this baseline is established, multi-shot experiments can be conducted more effectively, allowing clearer interpretation of the effects of repeated exposure.

To start simple, we first consider a single layer on a non-absorbing substrate.[63] Upon exposure to a single-shot laser pulse, the layer can absorb energy, heat up, reach its melting point, and subsequently resolidify or show other forms of damage, such as ablation (i.e., material removal). The specific damage mechanisms that arise depend on both the material properties and the characteristics of the incident light. Even within a single sample, varying the incident laser fluence F can lead to distinctly different outcomes. To capture this, we classify the observed damage into three main fluence regimes:

- **Low** fluence regime: The fluence of the material is too low to induce any *measurable* permanent fluence effects.
- **Pre-ablation** fluence regime: The laser pulse induces permanent changes in the material without causing full ablation. Although structural or morphological modifications occur, there is no complete removal of the layer from the substrate. It is important to realize that the difference with the low fluence regime also depends on how accurately we can measure these permanent changes. It is, therefore, not unthinkable that in some cases where there appears to be no damage, more sensitive or precise measurement equipment would show some form of damage after all.
- **High** fluence regime: Here, *full ablation* will occur, which is the rapid removal of material over the entire layer thickness.

26 March 2026 13:26:42

As measured and presented in our previous work,[23,26,27,46] in the pre-ablation fluence regime, morphological changes can already occur. These include phenomena, such as spallation, surface cracking, nanovolcano formation, delamination/folding, and top-layer ablation, as is shown in Fig. 5.

The direct cause of this morphological change is usually the redistribution of stresses, often caused by melting and resolidification into a different (crystal) structure and/or orientation. Here, the ultrafast pulse induces fast melting. Apparently, enough atomic mobility is induced, leading to a changed average grain size and structure after resolidification. This can be measured by electron backscatter diffraction (EBSD), which has a high spatial resolution and is very surface sensitive. This makes it one of the few inspection methods well-suited for detecting structural changes in nanometer-thick layers. Figure 6 illustrates the structural evolution across various positions within a single-shot laser illuminated site on an 8 nm thick film of ruthenium using maps of grain orientations. Due to the (Gaussian) beam profile, the local fluence is different for all different EBSD-map positions. Because of this, different stages of this damage and resolidification are apparent.

© Author(s) 2026

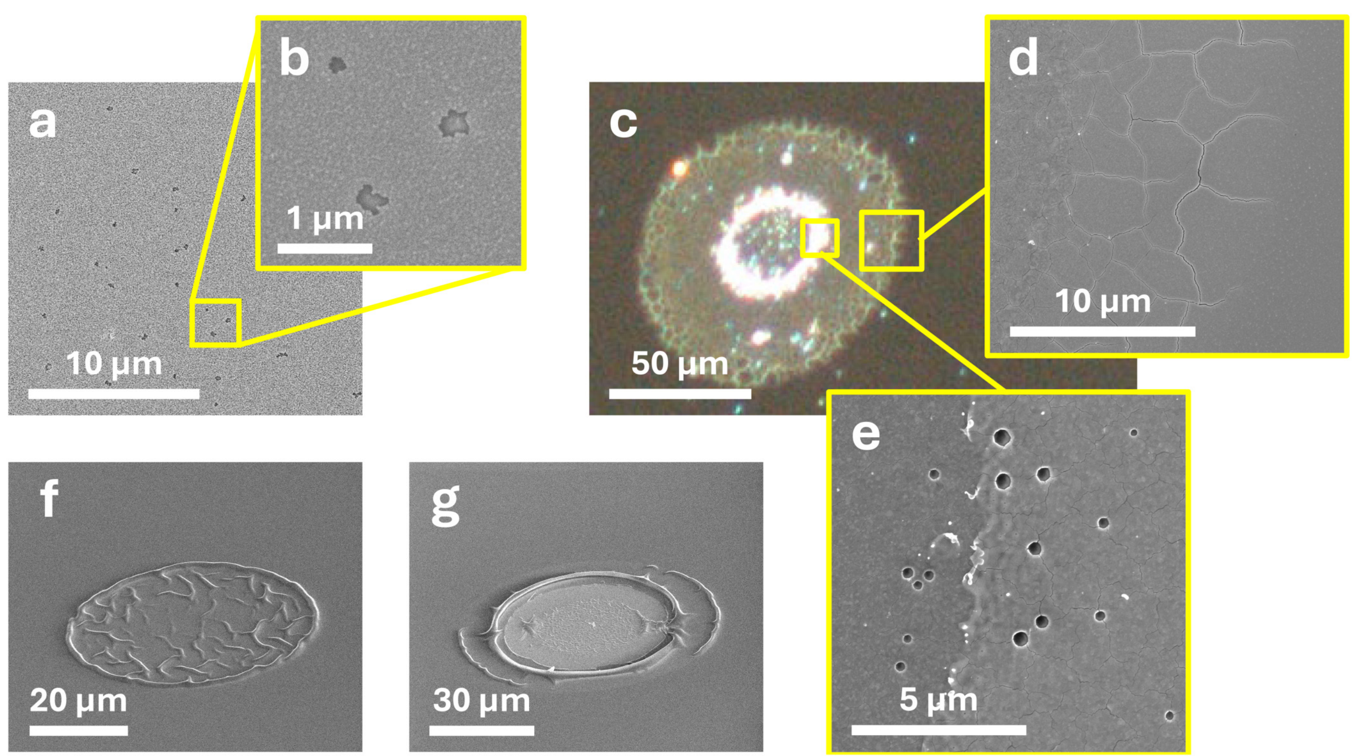

FIG. 5. Several SEM images and one optical dark field image of pre-ablation morphological changes obtained in different materials: (a) and (b) spallation of 20 nm Al on borosilicate glass. (c) is an optical microscopy dark field image of a damaged 20 nm thick layer of ruthenium on borosilicate glass. (d) and (e) are SEM images of the zoomed in version of parts of (c), showing cracking of the surface and nanovolcano formation, respectively. (f) shows delamination/folding and (g) top-level ablation of 100 nm amorphous carbon (aC) on Si. (f) and (g) are taken under a 52° tilting angle. All samples are illuminated by a single 400 nm ≈45 fs pulse with a ≈75 μm FWHM Gaussian beam profile.

26 March 2026 13:26:42

The EBSD scans clearly indicate that the melting threshold has been reached, leading to increased atomic mobility within the material. This not only alters the grain structure but also gives rise to additional morphological changes, as illustrated in Fig. 5. In the context of light-induced damage to optical components, such modifications might not be classified as catastrophic. However, in the semiconductor manufacturing industry—where sub-nanometer precision is critical, these seemingly minor sub-wavelength irregularities, such as material loss (spallation and cracking) or deformations (e.g., local density changes), are indeed catastrophic. Notably, the pre-ablation changes observed here already exceed the sub-nanometer tolerances required in semiconductor manufacturing and can, therefore, be considered catastrophic within this context.

It is not only flat films, but also often structured topographies that are exposed to the intense light sources used for metrology. When these nanostructures are irradiated with a fluence within the pre-ablation regime, where melting occurs, their surface topography can undergo significant changes. This is demonstrated in Fig. 7, which shows a SEM image and various AFM scans of a silicon grating after single-shot laser illumination. Even in this pre-ablation regime, the original line profiles of the gratings are substantially deformed. These modifications occur before any material is fully removed and include progressive deformation with increasing fluence: lines become rounded, their height increases, followed by flattening with a small "double period" structure, and ultimately, a complete inversion where peaks transform into valleys and vice versa.[23] In addition to these morphological changes, the observed topographical evolution confirms that melting has been reached in this regime. Such deformations are particularly detrimental in the context of nanolithographic device manufacturing, where precise feature geometry is essential. Therefore, reaching the melting threshold, which enables extensive and fast mobility of material, needs to be avoided at all costs. Supplementary Videos 1–3 in the supplementary material are made available, which show deformations of several gratings etched in silicon when illuminated by single 400 nm pump pulses with increasing fluences. These pulses are polarized parallel to a 600 nm period and a 50% duty cycle grating (Video 1 in the supplementary material), polarized perpendicular to grating lines with the same period and duty cycle (Video 2 in the supplementary material), and polarized perpendicular to grating lines with a 980 nm period and a 50% duty cycle (Video 3 in the supplementary material).

© Author(s) 2026

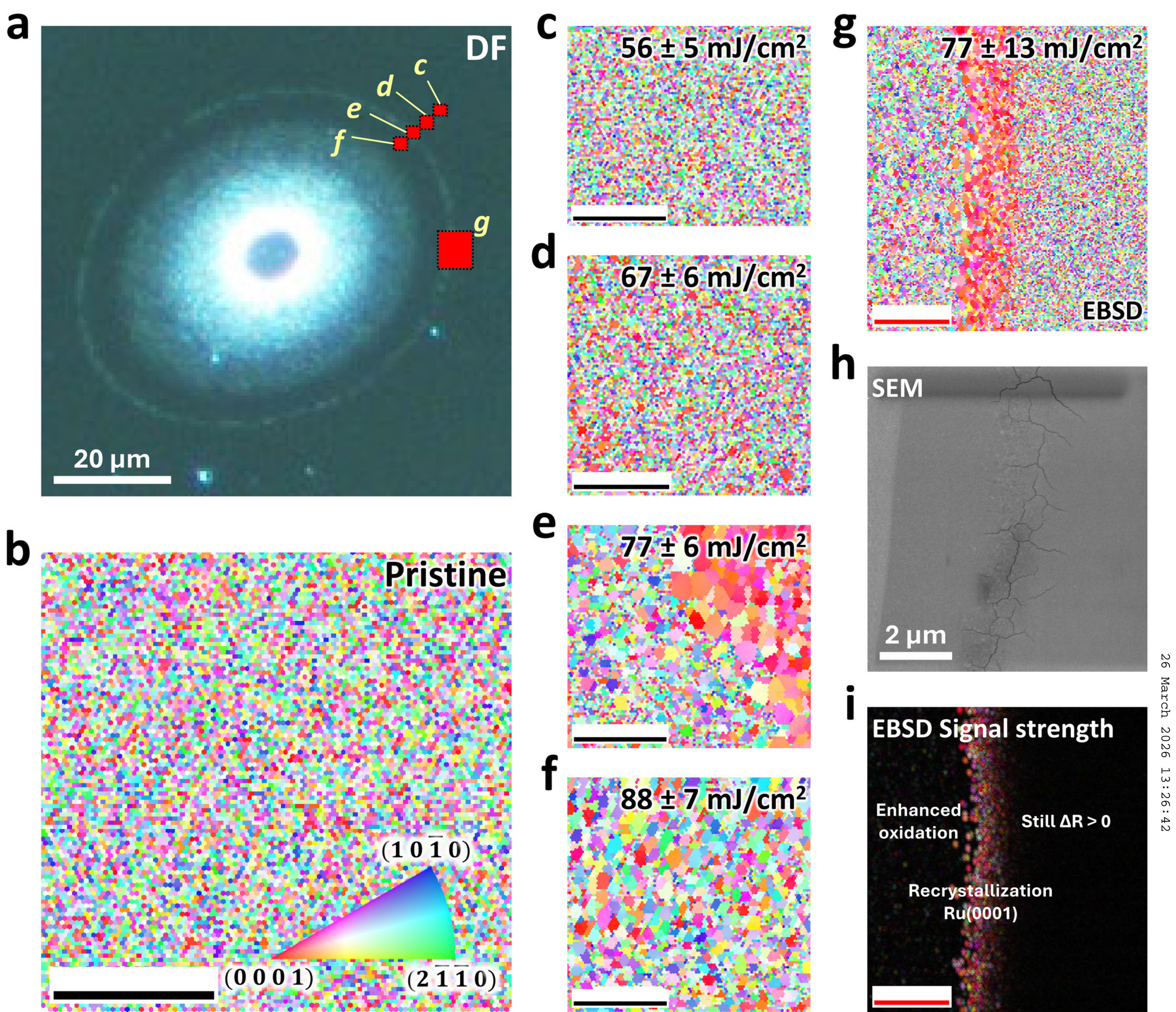

FIG. 6. (a) Dark-field microscopy image of a single-shot-illuminated site of an 8 nm thick layer of ruthenium on borosilicate glass. The red rectangles indicate the locations of the EBSD-maps (c)–(g). (h) and (i) are the SEM and EBSD signal strength images of (g). The local fluences of the EBSD maps are below the threshold fluence for nanovolcano formation ($F_{local} < 104\,mJ/cm^2$). (b) is a EBSD-scan of a pristine site. At all other scans, the local fluence is in the pre-ablation fluence regime, where $\Delta R > 0$ (see Sec. II C 3 and Fig. 8). The average values for F_{local} of each map are indicated at the corresponding EBSD image. The EBSD images are the inverse polar maps, which show the crystal direction, which is the direction normal to the sample. Each color corresponds to the direction in the range between (0001), (10$\bar{1}$0), and (2$\bar{1}\bar{1}$0) according to the triangle legend. The black and red scale bars are 1 and 2 μm wide, respectively. As is shown in the SEM image (h), cracks are formed. Around these cracks, the Ru has settled mostly in the (0001) orientation, which is its lowest surface-energy plane[64] (p. 91). For fluences higher than at the crack formation, enhanced oxidation of Ru has occurred. Reproduced from Abram *et al.*, J. Appl. Phys. **136**, 245305 (2024). Copyright 2024 Author(s), licensed under a CC BY 4.0 License.[27]

3. Direct inspection

As previously mentioned, structural changes can be detected using EBSD. However, this technique is often impractical for use in nanolithography due to its long acquisition times, which are required to generate high-quality EBSD maps. Given the demand for high-throughput inspection and the large wafer sizes—often containing more than 100 dies, EBSD becomes too slow and costly for routine monitoring.

26 March 2026 13:26:42

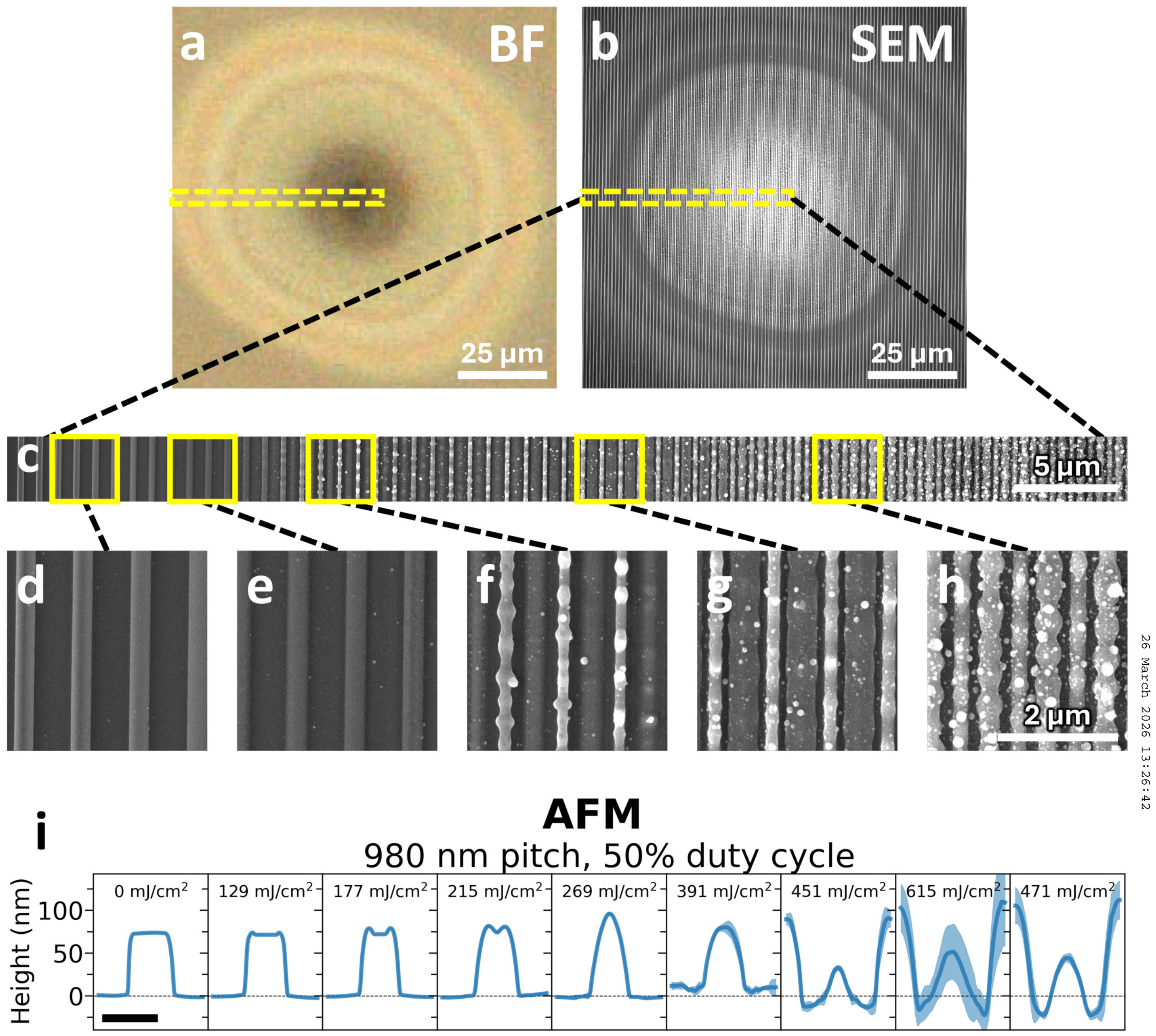

FIG. 7. (a) Optical bright field and (b) SEM image of a 980 nm period, 50% duty-cycle grating etched in silicon, illuminated by a single 400 nm pulse with a peak fluence of 1181 mJ/cm^2 and polarized perpendicular to the grating lines. (c) is the zoom in of the area outlined by the yellow dashed box in (a) and (b) and shows a "line scan" over an increasing local fluence when moving from left to the right of the image. Both the line scan and zoomed-in sections (d)–(h) show the progression of the grating line deformations. (i) are corresponding line scans across the deformed grating lines for increasing local fluences. These cross sections are derived from multiple 2D height maps obtained by AFM. Each height map covers 8 × 8 μm and consists of 1024 lines, where a variety of protocols, such as row alignment, masking, and removing the polynomial background, are implemented using Gwyddion software.[65] The black bar in (i) is 500 nm wide.

26 March 2026 13:26:42

Fortunately, permanent structural changes in the material typically also result in permanent optical changes. Alterations in the grain structure can lead to modifications in the effective refractive index compared to the pristine material. This enables a more efficient approach: by measuring the reflectivity of the material with a low-intensity probe beam, one can rapidly assess whether the melting threshold has been reached. This method can serve either as a quick tool for determining damage thresholds or it

© Author(s) 2026

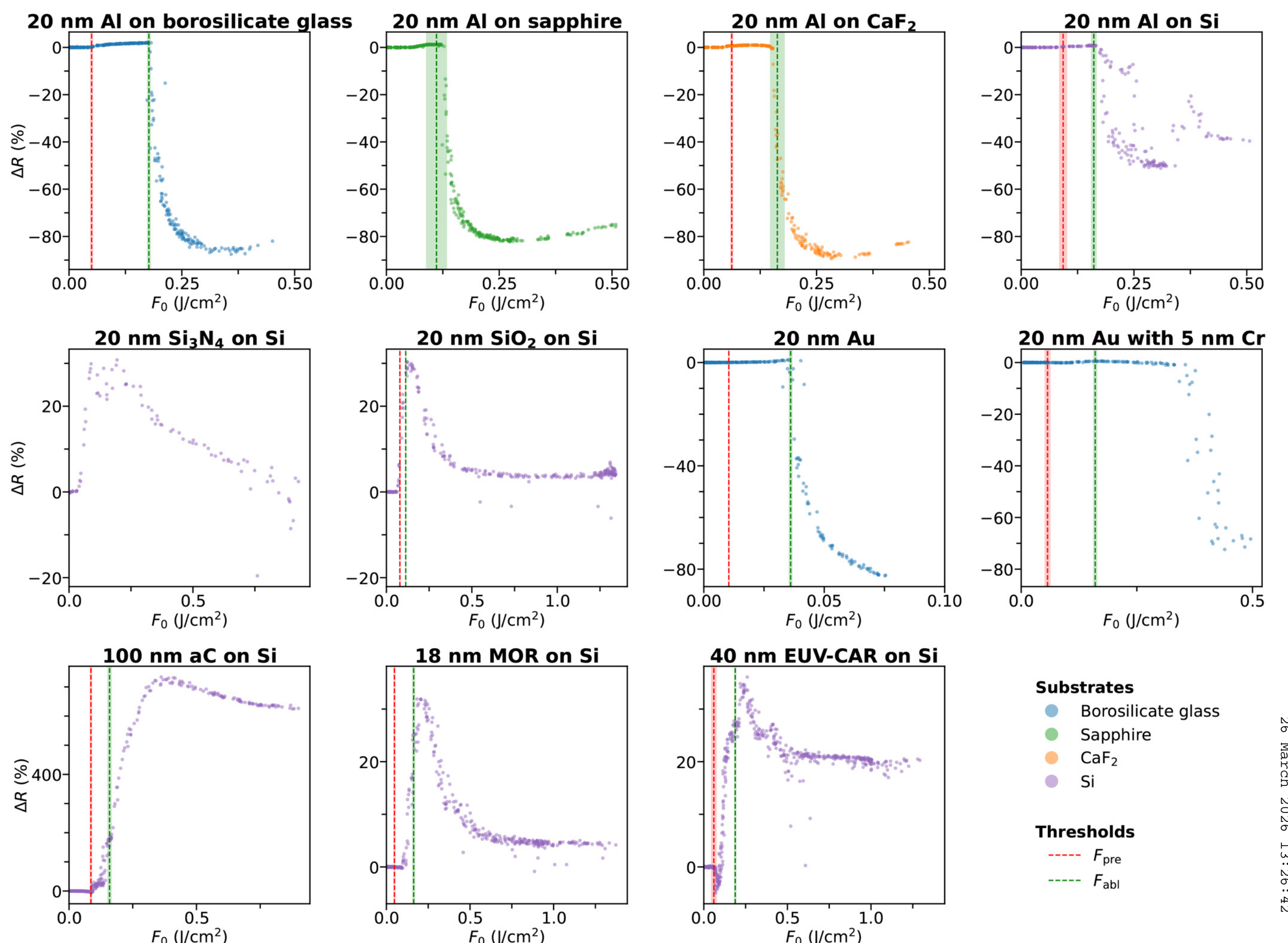

FIG. 8. Measured ΔR vs peak fluence F_0 for (a)–(d) 20 nm Al on various substrates, (e) 20 nm Si_3N_4, and (f) 20 nm SiO_2 on Si, and 20 nm Au on borosilicate glass without (g) and with (h) a 5 nm adhesion layer, and (i) 100 nm aC, (j) 18 nm MOR, and (k) 40 nm EUV-CAR on Si. The colors of the data points indicate the substrate, and the red and green vertical lines indicate the first measurable pre-ablation (F_{pre}) and the ablation threshold fluence (F_{abl}), respectively. Other found damage thresholds are not shown here. F_{pre} and F_{abl} are obtained from SEM and optical microscopy images. These data were not collected for the 20 nm Si_3N_4 layer.

26 March 2026 13:26:42

could be integrated as a real-time *warning* signal in the nanolithography machines.

Figure 8 provides selected examples of this effect in the form of measured relative reflection change ΔR curves of a 800 nm probe beam after illumination with a single-shot 400 nm pump pulse of peak fluence F_0 for different materials [Al, Si_3N_4, SiO_2, Au, aC, metal–oxide resist (MOR), and chemically amplified resist (CAR)] on different substrates (borosilicate glass, sapphire, CaF_2, and Si). ΔR is the relative reflection change compared to the measured reflection of the pristine material. As shown in the figure, ΔR can reach values from a couple to even tens of percent, depending on the material and its thickness.[66] By inspection of the samples with optical microscopy and SEM, and performing Liu-analysis on them,[67] several thresholds are obtained. Only the lowest fluence threshold F_{pre} (pre-ablation) obtained from these images, so at the onset of any measurable change, and the ablation threshold F_{abl} are drawn in the ΔR vs F_0 figures in Fig. 8. Here, F_{pre} coincides with the onset of the increase in ΔR. Confirming that probing ΔR in real-time is a good indication for reaching the onset of pre-ablation light-induced damage.

Often in the semiconductor manufacturing industry, stacks composed of several layers have to be considered. Even though this inspection technique is quick and easy to implement here, the “weakest” layer can be buried underneath opaque layers, invisible to the probe beam. While the light may not reach the buried layer, heat dissipated toward it can; if it has a lower melting temperature than the layers above it, this will cause damage. In this case, our direct ΔR inspection may not be sufficient. Next to ΔR inspection, we, therefore,

© Author(s) 2026

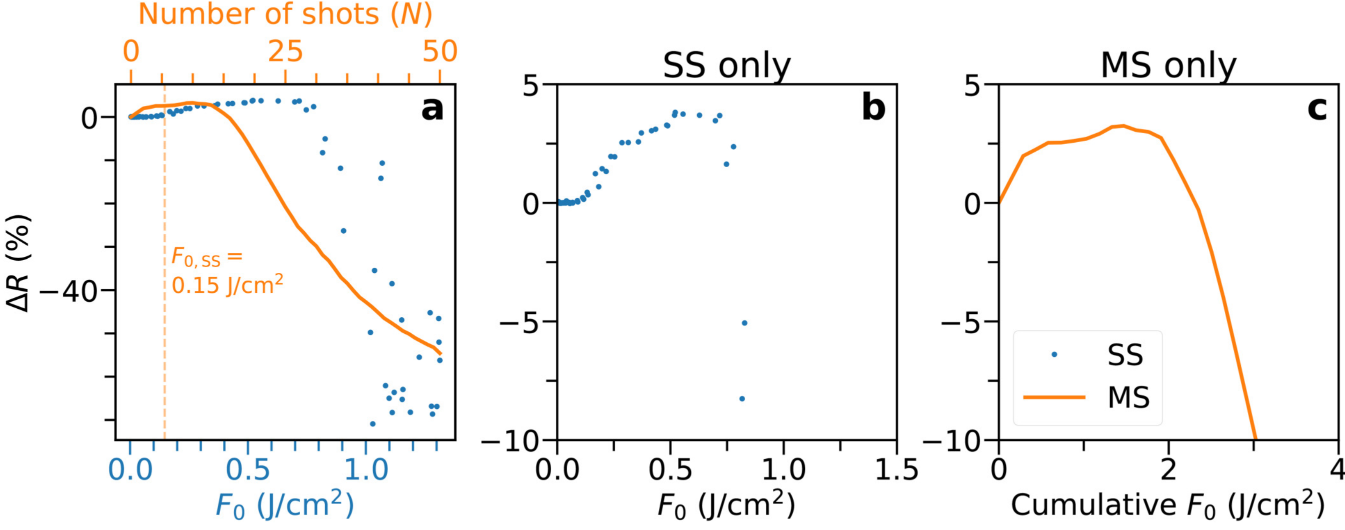

FIG. 9. Measured ΔR behavior under single-shot (SS) and multi-shot (MS) illumination of 8 nm ruthenium on borosilicate glass. (a) Measured ΔR vs SS peak fluence (blue), and vs the number of pulses (orange) for MS. (b) Vertically zoomed-in view of the SS data from (a), highlighting low-fluence behavior. (c) ΔR vs the cumulative fluence for MS illumination. For the MS measurement, the total number of pulses is 50, with an average peak fluence per pulse of $F_{0,SS} = 0.15\,\mathrm{J/cm^2}$, indicated by the vertical line in (a). Note that the MS data in (c) are zoomed in as well to allow an easy comparison with (b).

suggest implementing other inspection techniques as well, for instance, time-resolved ΔR-inspection upon quick illumination,[68,69] which is sensitive to the temperature of the (top of the) stack.

4. Multi-shot damage (S-on-1)

Moving closer to the actual use case, it is essential to consider the effects of multi-shot exposure on laser-induced damage [S-on-1[4] (pp. 167–168),[62] (p. 8)]. As demonstrated earlier, the single-shot relative reflectivity change ΔR depends on the (peak) fluence F. In multi-shot experiments, the damage threshold fluence per pulse $F_{0,s}$ is often lower than that observed for single-shot exposure. This suggests that even a single pulse can induce subtle, potentially undetectable, permanent changes within the material. Nevertheless, LID mechanisms, such as melting and resolidification, continue to take place under repeated exposure, with corresponding variations in ΔR. As shown in Fig. 9, the trend of ΔR as a function of (cumulative) peak fluence remains consistent between single-shot and multi-shot exposures. The key difference lies in the damage threshold value: although the peak fluence threshold that each pulse has for multi-shot exposure is lower, the cumulative fluence required to induce damge (so the peak fluence per pulse summed over the number of pulses) is actually higher as is shown in Figs. 9(a)–9(c). This implies that when transitioning to multi-shot exposure, the total energy dose delivered to the wafer can be increased. However, to avoid damage, the peak fluence per pulse ($F_{0,SS}$) must be reduced compared to the single-shot exposure limit. Importantly, since the $\Delta R(F_0)$ trend remains unchanged, this highlights the significance of ΔR measurements as a reliable and sensitive early warning signal in multi-shot regimes as well.

Figure 9 is included here to show that dividing the energy dose/photon budget over several pulses is beneficial. However, not only the total number of pulses N is relevant, but also the separation time τ between two consecutive pulses, and the pulse duration τ_p of each pulse will influence the total damage threshold, for example, by heat accumulation or incomplete carrier recombination. The complexity and vastness of this parameter space make it hard to predict what exact parameters to use for a desired energy dose. For metrology, it is essential to optimize the energy dose delivered per (average) time. This requirement arises from the need for sufficient signal strength while maintaining high processing speed needed for a high throughput of wafers, which makes this problem even more complex. However, as a first simplification step, one can separate the total number of pulses into different *regimes*: From single-shot, to double shots, to bursts—where multiple pulses illuminate the sample in rapid succession—and ultimately, to continuous irradiation.

Accurately predicting the laser-induced damage threshold (LIDT) is challenging even under single-shot conditions. Under multi-shot exposure, the problem becomes significantly harder. Next to the expansion of the parameter space by variables, such as the number of shots (N) and pulse separation time τ_p for "ideal" experiments, LIDT values at multi-shot exposure are very sensitive to, for instance, minor pulse-to-pulse variations, such as small variations in the peak intensity or pulse energy. This can already yield large discrepancies between predicted and measured LIDT values.

26 March 2026 13:26:42

© Author(s) 2026

Furthermore, N, τ_p, and τ (pulse duration) are often not independent but coupled, so straightforward extrapolations of LIDT fluence values (e.g., across different N, τ_p, and τ) are often unreliable. For practical operation, it would, therefore, make sense to focus on in-line inspection instead of theoretical predictions to determine the light-source parameters needed to operate below the damage threshold.

D. Indirect damage by light

In addition to the damage caused to materials directly by irradiation with light, the interaction of light and matter opens indirect pathways of degrading materials and their surfaces. Here, we define indirect light-induced effects as alterations caused by intermediate species that are generated through light–matter interaction some distance away from the affected material. Common examples of such species include radicals and ions that are created in light-induced plasmas or via the interaction of molecules with electrons liberated from surfaces as illustrated in Fig. 10. These particles have the ability to cause damage to materials located elsewhere in a lithography machine. For ionizing radiation in the vacuum ultraviolet (VUV) and extreme ultraviolet (EUV) regimes, this activation can take place as a result of the photoionization of molecules and surfaces and the light-induced breaking of molecular bonds. The strong interaction of EUV and VUV radiation with matter results in strong absorption of these wavelengths in solids, liquids, and gas environments. In a vacuum environment, EUV and VUV light can propagate over macroscopic distances, but significant rates of photoionization of molecules and electron emission from surfaces remain. As a result, the recent advances in nanolithography light source technology from operating wavelengths of 193 nm and above to the EUV wavelength of 13.5 nm have enhanced the importance of electron-induced damage pathways in nanolithography.

The electron-induced processes generated by EUV light in high vacuum introduce surface-related challenges in lithography technology, which are reminiscent of surface degradation in electron microscopy. Specifically, the deposition and accumulation of carbon on surfaces are a common result of the activation of organic background gas species via electron impact, leading to decreased transmission of photons.[70] Similarly, the activation of oxygen-containing species by electrons can result in the oxidation of the surfaces under study, changing the optical and electronic properties of the surface region.[71] For carbon deposition and oxidation, there is an effective mitigation strategy, which uses the same type of light- and electron-induced activation processes that cause contamination also for its removal. For this purpose, hydrogen gas in the pressure range of few Pa to tens of Pa is introduced into lithography setups. Upon exposure to EUV light, this background gas forms a plasma with EUV photons and photoelectrons as excitation sources.[72,73] The reactive species created by this plasma include hydrogen radicals and ions, which are capable of removing carbon[74,75] and oxygen from surfaces,[76] thus forming the basis of a successful strategy to minimize carbon and oxygen contamination of surfaces.

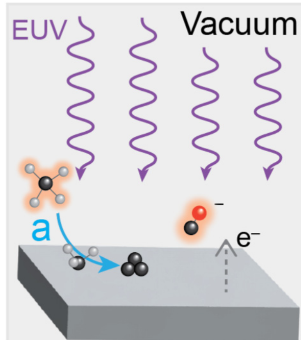

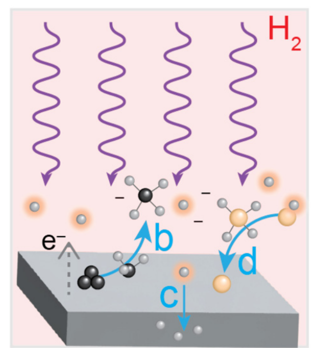

FIG. 10. Illustration of indirectly light-induced degradation processes: (a) carbon deposition, (b) etching by activated hydrogen species, (c) hydrogen incorporation and diffusion, and (d) redeposition of etched species.

The interaction of the EUV-induced reactive species with materials is neither limited to carbon and oxygen, nor to the immediate location where their activation takes place. Hydrogen radicals, for example, exhibit a high probability of being reflected from surfaces.[77,78] Thus, they do not only interact with directly exposed components, such as pellicles or lithography masks, but also with a variety of other coatings and construction materials. At the surfaces of popular construction materials, such as steel, titanium, or glass, the interaction with activated hydrogen can introduce several challenges, for example, related to the selective etching of chemical elements, the removal of passivating oxide layers, and the penetration of hydrogen into the bulk. The etching of materials by activated hydrogen can lead to the creation of volatile hydrides upon interaction with hydrogen plasma, for example, for Si[79] or Sn.[80] This process changes the surface composition and integrity of the etched layers but can also result in transport and redeposition of the etched elements onto functional surfaces, causing problems by altering layer properties, such as transmission.

The removal of protective coatings and the penetration of hydrogen into the bulk of construction materials after light-induced activation can introduce damage at depths that are not accessible via *direct* light-induced effects. The prime example of such a degradation process is hydrogen embrittlement, enhancing plasticity processes in materials and changing their microstructure,[81] thus accelerating the failure of affected materials, such as steel, titanium, and nickel-based superalloys.[82–84] Also, in this case, the role of the EUV light and the EUV-induced electrons is the generation of hydrogen radicals, which have been shown to accelerate the embrittlement process.[85] The various roles of secondary species in materials degradation highlight the importance of understanding the interaction of EUV light with matter also at intensities below the regime of direct photon-induced damage. The study of such indirect light-induced damage is, thus, crucial in lithography systems, especially when considering novel materials and devices in these harsh environments.

III. FUTURE AND PERSPECTIVE

A. Materials

Many different materials make up the semiconductor device stacks, each contributing a different function based on their

26 March 2026 13:26:42

© Author(s) 2026

electronic, thermal, physical, and chemical properties. These differing qualities contribute to the risks for LID, as the function of the material is the most important consideration. As illustrated in Fig. 1, even just considering the structures on the wafer during front end patterning becomes enormously complicated. The structures on the wafer consist of several layers of different materials in the form of thin films or patterned features. A clear understanding of the damage thresholds and damage mechanisms of these materials, stacks, and structures is necessary to evaluate the risks associated with powerful light sources. The essential building blocks—such as silicon serving as the transistor channel or copper forming metallic interconnects—are well established across technology nodes. However, the detailed composition, microstructure, and processing recipes of these materials often remain proprietary, differing significantly between device manufacturers and between technology generations. This serves as a strong motivation for fundamental investigation of LID for the materials and patterned structures on the wafer; in this way, LID can be a design consideration for chip manufacturers.

1. Important materials

The patterning stack is composed of different layers of "soft" material, which are applied on top and are the first to interact with incident light during lithography. These include photoresists, e.g., chemically amplified resist (CAR) or metal–oxide resist (MOR) used in both EUV and DUV lithography, variations of aC, antireflection coatings (organic and inorganic), planarizers and etching improvers, such as spin-on glass (SOG) and spin-on carbon (SOC). Owing to their composition, these materials generally exhibit relatively low light-induced damage threshold (LIDT). Therefore, understanding their damage mechanisms and how such damage may affect the underlying layers is crucial. Beneath the patterning stack, layers, such as oxides and nitrides, are commonly used as hard masks, liners,[86] or etch-stop barriers (see step 7 in Fig. 1). Examples include TiN, SiN, SiO_2, SiCN, and SiON, each serving specific roles in protecting and defining features during semiconductor fabrication. Extending throughout the device layers, metallic interconnects serve as vital pathways that link nanoscale devices to external circuitry. Materials, such as copper (Cu) and tungsten (W), are currently the materials of choice for these connections. In recent years, however, ruthenium (Ru) has attracted increasing interest due to its excellent conductivity at the nanoscale, making it a promising candidate to replace conventional interconnect materials. Transistors are fabricated using materials, such as silicon, silicon–germanium, polycrystalline silicon, and various dielectrics. Doping processes are commonly employed to establish the desired polarity within the semiconductor channel.

As the semiconductor industry moves beyond traditional silicon scaling, a new generation of materials is emerging to meet the demands of performance, power efficiency, and integration density. In advanced packaging, materials, such as thermally conductive adhesives, low-coefficient-of-thermal-expansion (CTE) polymers and composites, low-κ dielectrics, electromagnetic interference (EMI) shielding films, copper replacements (e.g., Co and Ru), and novel underfill compounds, are critical enablers of heterogeneous integration, chiplet architectures, and 3D stacking.[87] Beyond packaging, 2D materials, such as graphene, MoS_2, and WSe_2, are gaining attention for their atomic thinness and exceptional electrical properties, making them candidates for next-generation transistors and interconnects (see Sec. III A 2). III–V compound semiconductors (e.g., GaN and InGaAs) are being explored for high-speed and low-power logic, especially in RF and high-frequency applications. IGZO (Indium Gallium Zinc Oxide) is gaining traction in shaping 3D memory due to its high mobility and transparency. Ferroelectric materials, such as $HfZrO_x$, are enabling new memory technologies, such as FeRAM and ferroelectric FETs (FeFETs). Additionally, phase-change materials, spintronic materials, and topological insulators are being investigated for neuromorphic and quantum computing. These emerging materials are not merely extensions of Moore's Law—they are foundational to the *More-than-Moore era*, where functionality, integration, and new computing paradigms take center stage.[88]

2. 2D materials

A new class of materials, two-dimensional (2D) transition metal dichalcogenides (TMDs) are poised to play an outsized role in the next generations of semiconductor devices.[89–91] TMDs are stable as three-atom-thick layers in ambient conditions due to their crystal structure, which leaves no dangling bonds on their basal plane.[92] The most commonly studied of these are the semiconducting phases of the molybdenum and tungsten sulfides and selenides (MoS_2, $MoSe_2$, WS_2, and WSe_2), which have many attractive properties for nanoelectronics and optoelectronics. Notably, high carrier mobilities in the monolayer limit may give distinct performance advantages over silicon in ultra-scaled gate all-around (GAA) transistor structures, enabling further transistor shrink to few-angstrom nodes.[91,93] Second, direct bandgaps for monolayer TMDs make them attractive for applications where thin, atomically smooth, or flexible active layers are required for optoelectronics.[94,95] These prospects have led to a proliferation in research into fabrication and measurement of devices based on 2D TMDs.

Methods for producing monolayer films or flakes have developed significantly in the last decade, encompassing a wide range of exfoliation and deposition techniques.[96–99] Once made, these films are routinely characterized with laser spectroscopies and microscopies, including photoluminescence (PL), Raman spectroscopy, second harmonic generation (SHG), and pump–probe techniques.[100] Any researcher who has made laser-based measurements of 2D TMDs is intimately familiar with their sensitivity to LID. On the other hand, they are perhaps shockingly robust, considering their thickness, and can be made more so through encapsulation with 2D hexagonal boron nitride (hBN) layers or cryogenic cooling. However, most researchers in the field will have experience accidentally burning their samples under a laser tuned to the wrong power.

This sensitivity to laser damage has prompted several studies into the phenomenon, including power thresholds and damage mechanisms. Several studies have systematically studied how photoluminescence and Raman spectra change as a function of laser exposure, reaching the conclusion that under ambient conditions, water and oxygen ad- and desorption play a critical role in altering photoluminescence from neutral, charged, and defect-bound

26 March 2026 13:26:42

© Author(s) 2026

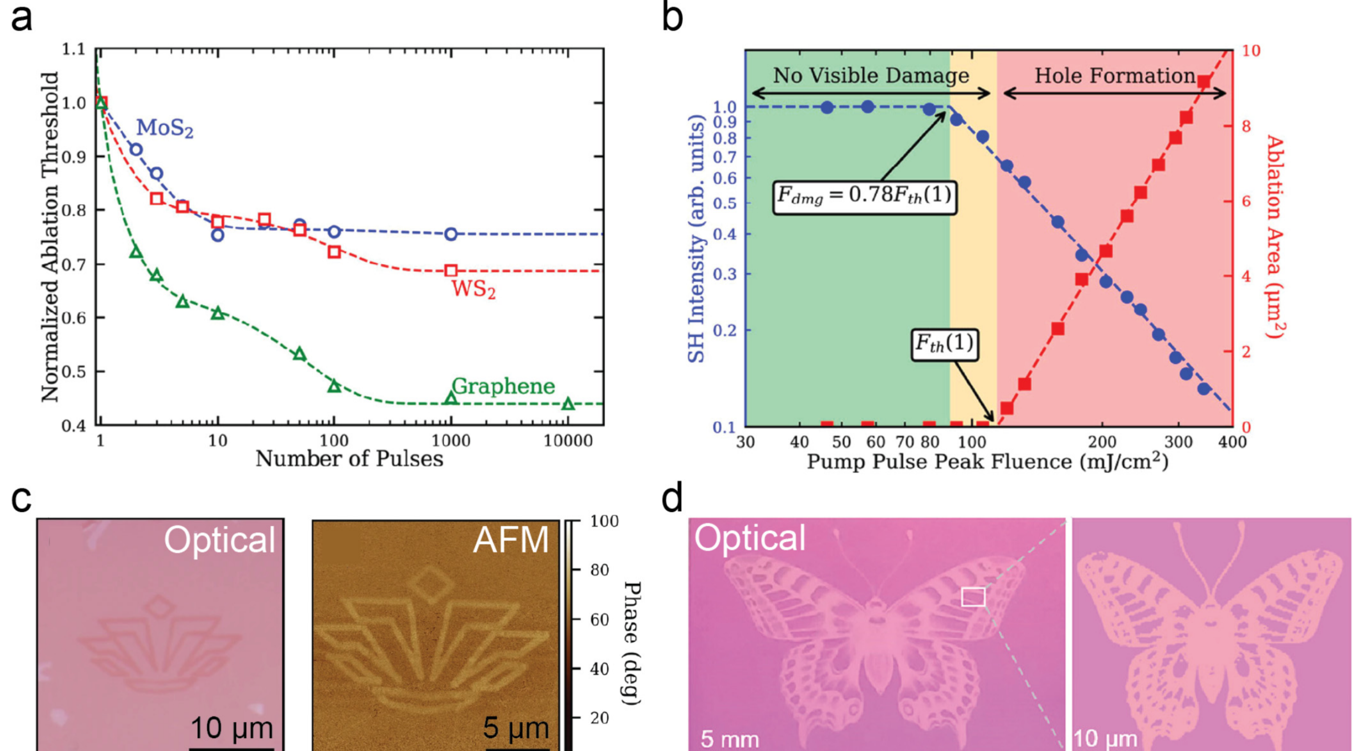

FIG. 11. (a) Normalized ablation threshold for different monolayer 2D materials damaged with different pulse numbers. (b) Damage threshold of monolayer MoS_2 with pump pulse fluence as measured by second harmonic generation (SHG) and ablation area. (a) and (b) Adapted from Solomon *et al.*, AIP Adv. **12**, 015217 (2022). Copyright 2022 Author(s), licensed under a CC BY 4.0 License.[105] (c) Optical and AFM images of MoS_2 patterned with a fs pulsed laser. Adapted from Solomon *et al.*, Sci. Rep. **12**, 6910 (2022). Copyright 2022 Author(s), licensed under a CC BY 4.0 License.[106] (d) Optical images of a MoS_2 film patterned with a $\lambda_{excitation} = 532$ nm ps-pulsed laser. Adapted with permission from Poddar *et al.*, Nano Lett. **22**, 726 (2022). Copyright 2022 American Chemical Society.[107]

26 March 2026 13:26:42

excitons.[101–104] These processes, however, may be irrelevant in many device applications where a TMD layer will be encapsulated by vacuum-deposited dielectric or metal layers.

In contrast to studies that explain phenomena of changing spectral signatures during routine Raman and photoluminescence measurements with continuous wave (CW) lasers, others have sought to understand how highly energetic, pulsed lasers can lead to irreversible damage and ablation. Solomon *et al.* presented two studies on how femtosecond (fs) laser pulses lead to damage and eventually ablation of TMD monolayers.[105,106] In single and multi-shot experiments, they identified MoS_2 as a particularly robust material against pulsed laser damage, with a saturation in the damage threshold value with as few as 10 pulses and a single-shot ablation threshold of 111 mJ/cm^2 (800 nm, 160 fs pulse duration) [Fig. 11(a)].[105] Furthermore, they studied how the substrate impacts the ablation of monolayer MoS_2 and found, remarkably, that the biggest determining factor is the intensity enhancement (or reduction) of the laser radiation at the MoS_2 layer.[106] This is the result of the boundary conditions of the electromagnetic field that require the field polarized parallel to the surface to be small. This allowed for ablation threshold tuning over an order of magnitude between MoS_2 on an Au film (least enhancement) and a distributed Bragg reflector (DBR, highest enhancement). Through SHG, photoluminescence, and Raman spectroscopy, they also identified a pre-ablation regime where the crystal is damaged through localized defects as shown by reduced intensity of characteristic SHG and PL peaks [Fig. 11(b)]. Raman spectra, however, show a more complicated picture where a combination of defects, strain, and doping may all be at play in altering MoS_2 before ablation can occur.[105] Further study is, therefore, warranted into the onset and mechanism of laser induced damage, especially in controlled atmospheres.

Several research groups have applied their experience in damaging 2D TMDs with laser radiation for direct-write optical patterning. Laser patterning has several advantages over other lithographies, notably the elimination of resists and solvents in patterning, which are known to have detrimental effects on TMD devices and fundamental properties. Solomon *et al.* extended their studies of pulsed laser damage to explicit patterning, showing ablated lines of ≈ 500 nm, slightly below the diffraction limit of their optics; this shows the high intensity dependence of ablation [Fig. 11(c)].[106] Additionally, Poddar *et al.* used a picosecond pulsed

© Author(s) 2026

532 nm laser to pattern arbitrary shapes and transistor channels into MoS_2 films, achieving submicrometer resolution [Fig. 11(d)].[107] They could also use their approach to disentangle the effects of different processing steps in conventional, resist-based lithography on TMD devices, showing that solvent exposure during development and resist removal is the most detrimental one. Their approach, however, used contacts patterned separately and transferred to the TMD film, which may not offer facile adoption routes in semiconductor manufacturing. Other studies have also shown direct laser patterning, for instance, in defining localized defect sites where etch pits can nucleate, followed by chemical vapor deposition (CVD) growth of a different TMD to yield lateral heterostructure arrays.[108,109] Resolution limits notwithstanding, such approaches may find application in semiconductor devices where device scale is not important, but other properties of 2D materials are advantageous, for instance, in back end of line (BEOL) integrated devices,[110,111] sensors,[112] or photonics.[113,114]

This collection of studies of laser damage and patterning of 2D TMDs begs the questions: How far can the resolution and fidelity be pushed, what are the potential challenges or drawbacks, and what are the prospects of direct laser writing for the semiconductor industry? The resolution of a laser-based approach will ultimately be governed by the optical diffraction limit and thermal diffusion, and thus the combination of laser wavelength, optical components, and material properties. The shortest wavelength used for direct laser writing of 2D TMDs reported so far has been 532 nm, used by Poddar *et al.* to create submicrometer patterns in MoS_2 films.[107] In addition, Cho *et al.* used a 308 nm excimer laser through a mask to directly ablate 2D MoS_2 films and make patterns with resolution down to 600 nm.[115] As yet, it is unclear how the damage threshold scales with photon energy, this will itself be a compelling area of study. However, there is also an opportunity to seek analogies for photolithography with incoherent light deeper into the UV. Only few studies have examined the effects of light with wavelengths lower than 300 nm, and for the most part, the damage reported is only subtle—a few defects introduced into an otherwise intact crystal.[116–118] Pushing these direct writing approaches to the ultimate resolution limits of course suggests exploring EUV-induced material damage. Few reports have explored EUV-induced damage to 2D TMDs; however, we suggest it as a fruitful avenue for future study, particularly in scanner-relevant conditions with plasma or gas discharge produced EUV light.

B. Measuring and fabrication techniques

1. Use LID for nanolithography

Currently, structures on a wafer are fabricated by depositing a layer, applying a resist, and using an etching process (see Fig. 1). Light is selectively projected onto the resist layer, triggering a chemical reaction. Subsequent etching removes exposed (or the non-exposed) portions of both the resist and the underlying layer, effectively transferring the desired pattern into the material (see Fig. 1). The use of resists, however, introduces additional complexity. The design of effective resists is highly dependent on the illumination wavelength.[119,120] As semiconductor manufacturing pushes toward ever-smaller nodes with higher numerical apertures (NAs), resist films must become thinner to preserve resolution and reduce aspect ratio constraints. However, this thinning introduces significant challenges, including increased stochastic effects and heightened sensitivity to shot noise, which collectively threaten pattern fidelity and yield. Moreover, delivering the required dose to the resist within a shorter timeframe increases the local (peak) intensity, making the resist layer especially vulnerable to light-induced damage. Eliminating the deposition and development of the resist layer is, therefore, desirable. If the light–matter interaction can be precisely controlled and tuned, *light-induced patterning* may enable novel fabrication approaches, reaching patterning of (sub)-diffraction-limited structures.[121] Consequently, alternative strategies for *resistless patterning* are currently under investigation. Here, light will directly shine onto the layer in a desired pattern, without the use of a resist layer. There are roughly two ways of resistless patterning: *Direct removal* of material with light and *area-selective modification* of materials (e.g., cross linking, changing the material properties, defect engineering in 2D materials, area-selective deposition, resistless, and atomic lithography).

Direct removal[122] is already widely used in the fabrication of microcircuits, for instance, in the fabrication of photonic integrated circuits.[123] Here, material is locally ablated, creating a pattern. The drawback of this technique is the difficult depth control and collateral damage. When a layer is deposited onto a second layer that is more susceptible to LID, it is hard to only remove the top layer. Furthermore, the ablation edges are often steep and relatively high, which makes this process hard to implement for small nanostructures. Here, area-selective modification of the material might be a more suitable patterning method. With this method, more subtle material changes are locally induced into the material by light. Often, an additional etching and/or deposition step is needed, but it is shown that high resolution structures can be fabricated this way.[28,124] Because there is no need to operate in the ablation regime, no debris is formed.

26 March 2026 13:26:42

An example of a material on which this technique can be deployed is ruthenium, which is a material of great interest for semiconductor device manufacturing. Where the resistivity of, for instance, copper and tungsten increases when the dimensions of conducting lines become smaller,[125–127] ruthenium (Ru) has appeared as a suitable alternative because of its good nanoscale conductivity.[128,129]

Ru can be patterned by localized heating of the material with a laser, which causes local *enhanced oxidation* and, therefore, produces a thicker ruthenium oxide (RuO_2) layer likely in the rutile phase.[28,64] In contrast to the Ru metal and its approximately 0.5 nm thick native oxide, this thicker oxide is resistant to dissolution by NaClO and can, thus, act as a protective layer. NaClO etching after laser exposure, thus, only removes the regions without the protective light-induced oxide. Since this light-induced oxidation is a thermally driven process, the ruthenium must exceed a threshold temperature for a short duration, meaning that thermal diffusion ultimately limits the resolution of the achievable structures. Nevertheless, even single-shot illumination with pulses as short as ≈ 45 fs has been demonstrated to cause enhanced oxidation on thin Ru layers (see Fig. 12). Moreover, in multi-shot experiments, irradiation with spot sizes as small as $2\,\mu$m has been shown to be capable of printing structures of 500 nm in width, surpassing the diffraction limit.[124] Thus, by employing thin layers, ultrashort

© Author(s) 2026

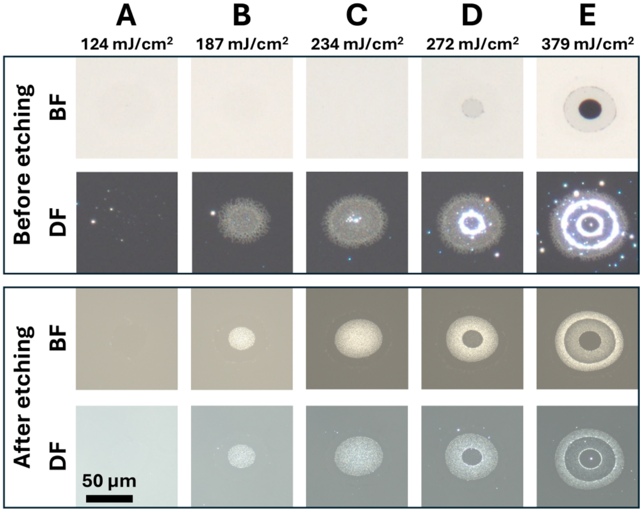

FIG. 12. Optical bright-field (BF) and dark-field (DF) images of five sites (A–E) on a 20 nm ruthenium film on borosilicate glass after illumination by a single 400 nm, ~45 fs pulse with a ≈75 μm FWHM Gaussian beam profile. Each site was exposed to a different (peak) fluence, ranging from 124 to 379 mJ/cm^2. The top two rows show BF and DF images before etching, and the two bottom rows show the same areas after etching in a NaClO solution. Where light-induced oxidation produced a sufficiently enhanced ruthenium-oxide layer, the oxide formed a protective layer that prevented dissolution of the ruthenium layer during NaClO etching.

pulses that promote rapid heating, and tightly focused beams, the resolution loss caused by heat diffusion can be minimized.

Obtained optical microscopy images showing this special way of patterning are shown in Fig. 12, providing a comparison of five sites on 20 nm Ru on borosilicate glass, illuminated by a single-shot ≈ 75 μm diameter (FWHM) Gaussian beam with different (peak) fluences (sites A–E). For all sites, four images were taken: Optical bright- and dark-field images before and after submerging the sample into NaClO (etching). For site A, the peak fluence of 124 mJ/cm^2 is too low to form a sufficiently enhanced RuO_2 layer to prevent dissolution in NaClO, whereas for B and C, a sufficiently enhanced oxide layer is formed. Where the local fluence exceeds the threshold fluence for enhanced oxidation ($F_{local} > F_{ox}$), ruthenium remains on the substrate after etching, as can be seen from the BF and DF images of the etched sites B and C in Fig. 12. For even higher (local) fluences, pre-ablation damage occurs in the form of top-level ablation,[16,27] where only the top part of the ruthenium layer is ablated. On the remaining Ru, the protective RuO_2 has not been sufficiently formed, presumably because by the time the top layer has ablated, the temperature of the remaining Ru was too low to allow significant oxidation. This explains why there still is ruthenium present in the center of site D before submerging the sample in NaClO, but not after, resulting in a ring-shaped Ru layer that remains on the substrate. Since the full-ablation threshold is reached in site E, a double ring-like structure remains after etching (since the ablation edge is still present).

For this measurement on 20 nm Ru, containing hundreds of illuminated sites of various (peak) fluences, a Liu-analysis[67] has been carried out for all four optical microscopy images. From this analysis, several threshold fluences (F_{th}) are obtained, including the fluence threshold to generate a protective RuO_2 layer sufficiently thick to prevent etching by NaClO, F_{ox}. All four Liu-plots are shown in Fig. S4 of the supplementary material, and only the Liu-plot obtained from optical bright-field microscopy images of the ruthenium after etching is selected to show in Fig. 13(a). In this figure, the fitted lines are obtained by an automated ellipse fitting procedure[130] from which a threshold fluence F_{th} is obtained.

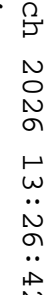

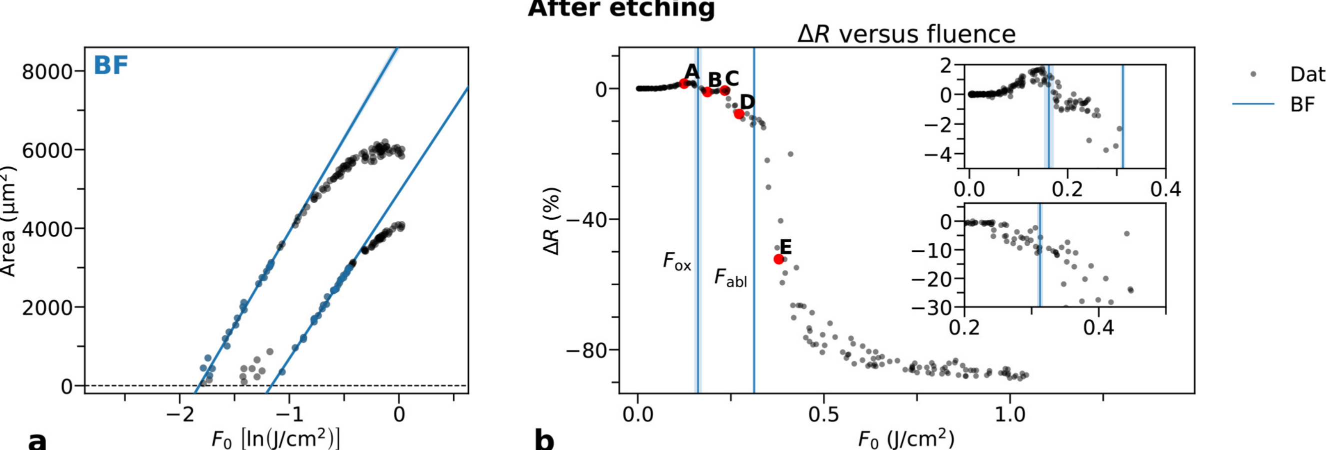

FIG. 13. Liu-plot (left) and ΔR vs peak fluence F_0 (right) of 20 nm ruthenium on a 0.5 mm borosilicate glass substrate. (a) is obtained from bright-field (BF) optical microscopy images after etching the sample where only the material covered by a protective layer of light-induced RuO_2 remains on the substrate, which occurs where the local fluence exceeds F_{ox}. This fluence threshold and that of ablation (F_{abl}) obtained by the Liu-plot are drawn as vertical lines in (b). A complete set of Liu-plots of both BF and dark-field (DF) optical microscopy images taken before and after etching is shown in Sec. III of the supplementary material.

© Author(s) 2026

The two values for F_{th} are drawn as vertical lines in Fig. 13(b) and represent the onset of sufficiently enhanced oxidation (F_{ox}) and the ablation fluence threshold (F_{abl}). Figure 13(b) shows the *in situ* measurement of ΔR vs the peak fluence F_0, where the illuminated sites A–E, as shown in Fig. 12, are indicated accordingly. $F_{ox} = (162 \pm 10)\,\mathrm{mJ/cm^2}$ is obtained from the DF images after exposing the sample to NaClO. It coincides with a small drop in $\Delta R(F)$, caused by the oxidation of Ru, which lowers the reflectivity as is confirmed with transfer-matrix method calculations.[47,131] Since F_{ox} depends on the stack composition and layer thickness, this drop in $\Delta R(F)$ can be used as an *in situ* probe of the successful formation of an oxide layer.

IV. RECOMMENDATION AND CONCLUSION

A. Signaling and predicting LID

A key takeaway of this perspective paper is that damage is not just limited to ablation. As discussed in Secs. II C–II D, *critical damage* can already occur below the ablation threshold fluence, for instance, when reaching the melting temperature. Here, even when exposed to an (ultra)short light pulse, already enough *mobility* in the atoms/molecules in the layer can be induced, leading to permanent structural and morphological changes in grain size, phase changes (crystalline vs amorphous), and surface deformations. All these effects modify the optical response, because changes in the grain structure, for example, will alter the effective refractive index directly by the effect that they have on the conductivity (see Sec. II C 3). Deformations, in, for instance, the shape of gratings when reaching the melting temperature (see Fig. 7), will directly affect the amount of specularly reflected light.

One also needs to be able to *measure* this "onset of damage." As discussed in Sec. II C 3, these light-induced changes can easily be probed by a (weak) probe beam as is experimentally shown in Fig. 8. This is fairly easy to implement, resulting in a "warning signal." Although this inspection method often uses visible light, extending the wavelength beyond the visible could very well improve the detection sensitivity and selectivity. Infrared or even THz radiation[132] could be used to probe the conductivity (change) inside, for example, doped semiconductor layers.

Even though inspection techniques to determine damage *in situ* may be useful, one could argue that observing damage means that one is already too late. However, this may not be true for all types of damage. Therefore, depending on the application and specifications of the material, one always has to define *when* damage is to be considered critical. If one probes the slightest change in optical properties, the same warning signal can still trigger very early, almost at the onset of damage, which, in some cases, may still be "on time." However, in the context of semiconductor manufacturing industry, minute light-induced material changes can already be considered critical.[46] In this regime, probing permanent optical changes is useful for quickly determining the light-induced damage threshold, but not for *in-line, real-time* inspection. To obtain a true early-warning signal, one can shift from measuring the "permanent aftermath" to probing the ultrafast electron dynamics during and immediately after laser excitation. The fast optical response driven by the electron temperature (T_e) can typically be detected at fluences far below any form of damage. However, measuring the reflectivity $R(T_e)$ will not only depend on T_e and the incidence fluence, but also on the material (i.e., its band structure). To extract the electron temperature from the measured $R(T_e)$ and calculate the reached lattice temperature from T_e is not that straightforward. Where for some materials theoretical models are developed,[17,69] it is always necessary to combine this with experimentally obtained calibration measurements. One could, for example, build an "electron response" library that correlates/lists $R(T_e)$ to light-induced damage threshold values.[54] One would then only need to keep the measured ultrafast light-induced reflection change under a pre-established value to avoid permanent damage. This approach will mostly apply to metals and semiconductors—which is appropriate, as these layers absorb directly and often constitute the weakest part of a stack and are most likely to damage first.

B. Conclusion

Semiconductor device manufacturing is an extremely dynamic industry. In this article, we highlight light-induced damage occurring in various environments, in different materials, and by using different light sources, typical for current and future technological developments. The semiconductor industry, however, is huge, and therefore, any attempt to be comprehensive is doomed to fail. Nevertheless, we feel we have given a glimpse into current and future challenges facing the industry when using present and future light sources, materials, and optical components. As novel materials, such as 2D layers, are adopted, and illumination sources may extend from the THz domain to beyond EUV with different temporal and spatial patterns, the parameter space governing damage-threshold fluences is expanding and will continue to grow in the near future. Consequently, defining *what* critical damage is and *when* the onset of it occurs cannot be done unambiguously across the entire parameter space. Because light-induced damage manifests in many ways throughout semiconductor manufacturing, fundamental science, combined with input from the semiconductor manufacturing industry itself, is key to solving fundamental challenges: both in overcoming unwanted critical damage and in beneficially exploiting light-induced damage.

26 March 2026 13:26:42

SUPPLEMENTARY MATERIAL

See the supplementary material for supporting content, including a *Light sources overview*, *Mathematical framework for light-absorption to heat transfer*, and additional *Ruthenium Liu-plots*, and Supplementary Videos 1–3 showing *grating-line deformations for increasing fluences*.

ACKNOWLEDGMENTS

The authors thank Klaasjan van Druten for his extensive discussions and mathematical assistance. We also extend our gratitude to Lorenzo Cruciani, Marnix Vreugdenhil, Dries van Oosten, Thomas van den Hooven, Amir Abdolvand, and Rolf Koole for their insightful discussions, and Nikolai Orlov and Erik Garnett for the EBSD-scans. Additionally, we would like to thank the technical support provided by Thomas Meijvogel, Igor Hoogsteder, Dylan Loozen, and Bob Drent and software support by Marco Seynen.

© Author(s) 2026

"Wafer damage control: Understanding and preventing light-induced material changes in optical measurement systems" (with Project No. 17963) of the research program High Tech Systems and Materials (HTSM), which is (partly) financed by the Dutch Research Council (NWO). The project is co-financed by ASML and ASM Laser Separation International (ALSI). Electron Backscatter Diffraction characterization is part of the project "Achieving Semiconductor Stability From The Ground Up" (with Project No. 19459), which is financed by the Dutch Research Council (NWO), Gatan (EDAX), Amsterdam Scientific Instruments (ASI), and CL Solutions.

AUTHOR DECLARATIONS

Conflict of Interest

The authors have no conflicts to disclose.

Author Contributions

Ester Abram: Conceptualization (lead); Data curation (lead); Formal analysis (lead); Investigation (lead); Methodology (lead); Software (lead); Validation (lead); Visualization (lead); Writing – original draft (lead); Writing – review & editing (lead). **Reynolds Dziobek-Garrett:** Conceptualization (equal); Formal analysis (equal); Investigation (equal); Methodology (equal); Validation (equal); Visualization (equal); Writing – original draft (equal); Writing – review & editing (equal). **Vina Faramarzi:** Conceptualization (equal); Methodology (equal); Resources (equal); Validation (equal); Writing – original draft (equal); Writing – review & editing (supporting). **Roland Bliem:** Investigation (equal); Methodology (equal); Writing – original draft (supporting); Writing – review & editing (supporting). **Paul Planken:** Conceptualization (equal); Funding acquisition (lead); Methodology (equal); Project administration (lead); Supervision (lead); Validation (equal); Writing – review & editing (equal).

DATA AVAILABILITY

The data that support the findings of this study are available from the corresponding author upon reasonable request.

REFERENCES

[1]N. Bloembergen, Phys. Today **54**(9), 56 (2001).
[2]F. J. McClung and R. W. Hellwarth, J. Appl. Phys. **33**, 828 (1962).
[3]P. V. Avizonis and T. Farrington, Appl. Phys. Lett. **7**, 205 (1965).
[4]D. Ristau, *Laser-Induced Damage in Optical Materials* (CRC Press, 2014).
[5]W. Rudolph, L. Emmert, Z. Sun, D. Patel, and C. Menoni, Proc. SPIE **8885**, 888516 (2013).
[6]J. R. Gulley, Proc. SPIE **7842**, 78420U (2010).
[7]M. Jupé, L. Jensen, K. Starke, D. Ristau, A. Melninkaitis, and V. Sirutkaitis, Proc. SPIE **7504**, 75040N (2009).
[8]L. Gallais, D.-B. Douti, M. Commandré, G. Batavičiūtė, E. Pupka, M. Ščiuka, L. Smalakys, V. Sirutkaitis, and A. Melninkaitis, J. Appl. Phys. **117**, 223103 (2015).
[9]B. Rethfeld, K. Sokolowski-Tinten, D. von der Linde, and S. Anisimov, Appl. Phys. A **79**, 767 (2004).
[10]M. F. Koldunov, A. A. Manenkov, and I. L. Pokotilo, Quantum Electron. **32**, 335 (2002).
[11]M. Vreugdenhil and D. van Oosten, Proc. SPIE **12726**, 1272609 (2023).
[12]M. Vreugdenhil, "Shedding too much light on semiconductors: An investigation on laser-induced damage and ablation in semiconductors," Doctoral thesis (Universiteit Utrecht, 2025).
[13]J.-Y. Natoli, L. Gallais, H. Akhouayri, and C. Amra, Appl. Opt. **41**, 3156 (2002).
[14]A. A. Manenkov and A. M. Prokhorov, Sov. Phys. Usp. **29**, 104 (1986).
[15]S. Shead, "The Dutch firm that investors are going wild over is now creating a machine that could redefine electronics," (2021); see https://www.cnbc.com/2021/12/10/asmls-high-na-euv-lithography-machine-is-set-to-transform-chipmaking.html (accessed June 28, 2024).
[16]I. Milov, V. Zhakhovsky, D. Ilnitsky, K. Migdal, V. Khokhlov, Y. Petrov, N. Inogamov, V. Lipp, N. Medvedev, B. Ziaja, V. Medvedev, I. Makhotkin, E. Louis, and F. Bijkerk, Appl. Surf. Sci. **528**, 146952 (2020).
[17]F. Akhmetov, I. Milov, S. Semin, F. Formisano, N. Medvedev, J. M. Sturm, V. V. Zhakhovsky, I. A. Makhotkin, A. Kimel, and M. Ackermann, Vacuum **212**, 112045 (2023).
[18]A. J. den Boef, Surf. Topogr.: Metrol. Prop. **4**, 023001 (2016).
[19]T. van Gardingen-Cromwijk, S. Konijnenberg, W. Coene, M. Adhikary, T. Tukker, S. Witte, J. F. de Boer, and A. den Boef, Light: Adv. Manuf. **4**, 453 (2023).
[20]Furthermore, in order to correct for intra-field fingerprints, which is the area within the scribe lanes covering the entire die after lithography, alignment markers within this field are also necessary.
[21]G. Zhang, M. Graef, and F. van Roosmalen, in *56th Electronic Components and Technology Conference 2006* (IEEE, 2006), pp. 151–157.
[22]M. M. Waldrop, Nat. News **530**, 144 (2016).
[23]E. Abram and P. Planken, Opt. Express **33**, 27839 (2025).
[24]K. Biesheuvel and P. Huberts, PhotonicsViews **21**, 48 (2024).
[25]G. Ren, H. Sun, T. Koike, K. Takabayashi, K. Nakagawa, N. Sugita, and Y. Ito, Ultrafast Sci. **5**, 0109 (2025).
[26]E. Abram, I. Milov, N. Orlov, K. van Druten, E. C. Garnett, and P. Planken, Opt. Express **32**, 4564 (2024).
[27]E. Abram, N. Orlov, E. C. Garnett, and P. Planken, J. Appl. Phys. **136**, 245305 (2024).
[28]L. Cruciani, M. Vreugdenhil, S. van Vliet, E. Abram, D. van Oosten, R. Bliem, K. van Druten, and P. Planken, Appl. Phys. Lett. **124**, 171902 (2024).
[29]L.-T. Tseng, P. Karadan, D. Kazazis, P. C. Constantinou, T. J. Stock, N. J. Curson, S. R. Schofield, M. Muntwiler, G. Aeppli, and Y. Ekinci, Sci. Adv. **9**, eadf5997 (2023).
[30]A small dielectric constant with respect to that of SiO_2.
[31]IEEE, "Roadmap IRDS 2024: Metrology," in *International Roadmap for Devices and Systems^{TM}* (IEEE, 2024).
[32]N. Park, D. Lee, L. Liu, X. Zhou, H. Su, D. Choi, W. Zhou, H. Spielberg, E. Megged, C. Dror, D. Shaphirov, Z. Liu, M. Ghinovker, D. Lee, H. Yeon, H. Kim, S. Park, B. Kim, H. Lee, and S. Lee, Proc. SPIE **12053**, 120530E (2022).
[33]C. Messinis, T. T. M. van Schaijk, N. Pandey, A. Koolen, I. Shlesinger, X. Liu, S. Witte, J. F. de Boer, and A. den Boef, Opt. Express **29**, 38237 (2021).
[34]*The Supercontinuum Laser Source: The Ultimate White Light*, 4th ed., edited by R. R. Alfano (Springer, Cham, 2022).
[35]P. Uebel, J. Köhler, M. H. Frosz, and M. Bergler, Proc. SPIE **13342**, 133420D (2025).
[36]M. Jupé, L. Jensen, A. Melninkaitis, V. Sirutkaitis, and D. Ristau, Opt. Express **17**, 12269 (2009).
[37]V. E. Gruzdev, J. Opt. Technol. **71**, 504 (2004).
[38]L. V. Keldysh, Zh. Eksp. Teor. Fiz. **47**, 1307–1314 (1964).
[39]A. Kaiser, B. Rethfeld, M. Vicanek, and G. Simon, Phys. Rev. B **61**, 11437 (2000).
[40]B. Rethfeld, Phys. Rev. Lett. **92**, 187401 (2004).

26 March 2026 13:26:42

© Author(s) 2026

[41]B. J. Demaske, V. V. Zhakhovsky, N. A. Inogamov, and I. I. Oleynik, Phys. Rev. B **87**, 054109 (2013).
[42]R. Fang, A. Vorobyev, and C. Guo, Light: Sci. Appl. **6**, e16256 (2017).
[43]A. Miotello and R. Kelly, Appl. Phys. A **69**, S67 (1999).
[44]P. Lorazo, L. J. Lewis, and M. Meunier, Phys. Rev. B **73**, 134108 (2006).
[45]K. C. Phillips, H. H. Gandhi, E. Mazur, and S. K. Sundaram, Adv. Opt. Photonics **7**, 684 (2015).
[46]E. Abram, *What Is Light-Induced Damage? Pre-ablation Regime Optical and Morphological Changes in Nanometer Thick Films and Grating Structures* (University of Amsterdam, 2025), p. 217.
[47]E. Abram, "Multilayers," version 1.0.0 (2024); see https://git.amolf.nl/Light-Matter_Interaction/multilayers.git.
[48]M. Born and E. Wolf, *Principles of Optics*, 6th ed. (Cambridge University Press, Cambridge, UK, 1980), pp. 51–70.
[49]M. G. M. M. Van Kraaij, "Forward diffraction modelling: Analysis and application to grating reconstruction," Doctoral thesis (Technische Universiteit Eindhoven, 2011).
[50]H. Zhang, S. A. Wolbers, D. M. Krol, J. I. Dijkhuis, and D. van Oosten, J. Opt. Soc. Am. B **32**, 606 (2015).
[51]B. Rethfeld, D. S. Ivanov, M. E. Garcia, and S. I. Anisimov, J. Phys. D: Appl. Phys. **50**, 193001 (2017).
[52]B. Wu and Y. C. Shin, Appl. Surf. Sci. **253**, 4079 (2007).
[53]B. Wu and Y. C. Shin, Appl. Surf. Sci. **255**, 4996 (2009).
[54]F. Akhmetov, N. Medvedev, I. Makhotkin, M. Ackermann, and I. Milov, Materials **15**, 5193 (2022).
[55]M. Kaganov, Sov. Phys. JETP **4**, 173 (1957).
[56]S. I. Anisimov, "Sov. Phys. Tech. Phys. **11**, 945 (1967).
[57]S. Anisimov, B. Kapeliovich, T. Perelman *et al.*, Zh. Eksp. Teor. Fiz. **66**, 375 (1974).
[58]F. Akhmetov, J. Vorberger, I. Milov, I. Makhotkin, and M. Ackermann, Opt. Express **32**, 19117 (2024).
[59]C. Dias, Int. J. Heat Mass Transfer **85**, 1075 (2015).
[60]N. Subani, F. Jamaluddin, M. A. H. Mohamed, and A. D. H. Badrolhisam, J. Phys.: Conf. Ser. **1551**, 012002 (2020).
[61]I. Milov, "Damage processes in ruthenium thin films induced by ultrashort laser pulses," Ph.D. thesis (University of Twente, Enschede, The Netherlands, 2020).
[62]International Organization for Standardization, "Lasers and laser-related equipment—Test methods for laser-induced damage threshold—Part 2: Threshold determination," International Standard ISO 21254-2:2011(E) (International Organization for Standardization, Geneva, Switzerland, 2011).
[63]Note that considering a freestanding layer is actually more complicated due to the induced stresses and traveling sound waves. Therefore, it has a lower threshold as well. However, such freestanding layers will not occur on wafers and are, therefore, not considered here.
[64]S. van Vliet, *Surface Chemistry of Ruthenium* (University of Amsterdam, 2025).
[65]D. Nečas and P. Klapetek, Cent. Eur. J. Phys. **10**, 181 (2012).
[66]Note that for a weakly reflecting initial state, ΔR can reach very high levels for fluences *above* the *ablation threshold* due to the exposure of the higher reflecting substrate, such as for the aC on silicon [Fig. 8(i)]. However, the pre-ablation ΔR value is much lower.
[67]J. M. Liu, Opt. Lett. **7**, 196 (1982).
[68]J. Hohlfeld, J. G. Müller, S.-S. Wellershoff, and E. Matthias, Appl. Phys. B **64**, 387 (1997).
[69]K. H. Bennemann, *Non-Linear Optics in Metals* (Oxford University Press, 1998), Vol. 98, pp. 225–230.
[70]M. Niibe, T. Harada, A. Heya, T. Watanabe, and N. Matsuo, AIP Conf. Proc. **2054**, 060010 (2019).
[71]M. H. Modi, S. Gupta, P. K. Yadav, R. Gupta, A. Bose, C. Mukherjee, P. Jonnard, and M. Idir, J. Synchrotron Radiat. **29**, 978 (2022).
[72]J. Beckers, T. van de Ven, R. van der Horst, D. Astakhov, and V. Banine, Appl. Sci. **9**, 2827 (2019).
[73]M. A. van de Kerkhof, A. M. Yakunin, D. Astakhov, M. van Kampen, R. van der Horst, and V. Banine, J. Micro/Nanopatterning Mater. Metrol. **20**, 033801 (2021).
[74]A. Dolgov, D. Lopaev, T. Rachimova, A. Kovalev, A. Vasil'eva, C. J. Lee, V. M. Krivtsun, O. Yakushev, and F. Bijkerk, J. Phys. D: Appl. Phys. **47**, 065205 (2014).
[75]C. Donnelly, R. McCullough, and J. Geddes, Diam. Relat. Mater. **6**, 787 (1997).
[76]T. Tsarfati, E. Zoethout, R. van de Kruijs, and F. Bijkerk, Surf. Sci. **603**, 2594 (2009).
[77]R. K. Grubbs and S. M. George, J. Vac. Sci. Technol. A **24**, 486 (2006).
[78]G. A. Melin and R. J. Madix, Trans. Faraday Soc. **67**, 2711 (1971).
[79]S. M. Gates, R. R. Kunz, and C. Greenlief, Surf. Sci. **207**, 364 (1989).
[80]D. Ugur, A. Storm, R. Verberk, J. Brouwer, and W. Sloof, Chem. Phys. Lett. **552**, 122 (2012).
[81]I. M. Robertson, P. Sofronis, A. Nagao, M. L. Martin, S. Wang, D. W. Gross, and K. E. Nygren, Metall. Mater. Trans. A **46**, 2323 (2015).
[82]J. Lee, in *Gaseous Hydrogen Embrittlement of Materials in Energy Technologies*, Woodhead Publishing Series in Metals and Surface Engineering Vol. 2, edited by R. P. Gangloff and B. P. Somerday (Woodhead Publishing, 2012), pp. 624–667.
[83]M. Louthan, G. Caskey, J. Donovan, and D. Rawl, Mater. Sci. Eng. **10**, 357 (1972).
[84]H. Yu, A. Díaz, X. Lu, B. Sun, Y. Ding, M. Koyama, J. He, X. Zhou, A. Oudriss, X. Feaugas, and Z. Zhang, Chem. Rev. **124**, 6271 (2024).
[85]H. G. Nelson, D. P. Williams, and A. S. Tetelman, Metall. Trans. **2**, 953 (1971).
[86]Liners or spacers are very thin layers that have multiple functions; e.g., they can act as protection, isolation, or enhancers of other layers. In interconnects, there is always a liner and a barrier between a metal and a dielectric layer. The barrier prevents diffusion of the metal into the dielectric, and the liner enhances the metalization of the interconnect.
[87]G. Haley, "Semiconductor engineering," (2024); see https://semiengineering.com/precision-under-pressure-navigating-increased-complexity-in-advanced-packaging/ (accessed October 20, 2025).
[88]"Beyond CMOS and emerging materials integration," in *IEEE International Roadmap for Devices and Systems* (IEEE, 2023).
[89]M. Chhowalla, D. Jena, and H. Zhang, Nat. Rev. Mater. **1**, 16052 (2016).
[90]C. Liu, H. Chen, S. Wang, Q. Liu, Y.-G. Jiang, D. W. Zhang, M. Liu, and P. Zhou, Nat. Nanotechnol. **15**, 545 (2020).
[91]Y. Liu, X. Duan, H.-J. Shin, S. Park, Y. Huang, and X. Duan, Nature **591**, 43 (2021).
[92]M. Chhowalla, H. S. Shin, G. Eda, L.-J. Li, K. P. Loh, and H. Zhang, Nat. Chem. **5**, 263 (2013).
[93]F. Gstrein, Proc. SPIE **PC12497**, PC1249704 (2023).
[94]K. F. Mak and J. Shan, Nat. Photon. **10**, 216 (2016).
[95]R. Dziobek-Garrett and T. J. Kempa, J. Chem. Phys. **160**, 200902 (2024).
[96]T. Zhang, J. Wang, P. Wu, A.-Y. Lu, and J. Kong, Nat. Rev. Mater. **8**, 799 (2023).
[97]T. H. Choudhury, X. Zhang, Z. Y. Al Balushi, M. Chubarov, and J. M. Redwing, Annu. Rev. Mater. Res. **50**, 155 (2020).
[98]F. Liu, W. Wu, Y. Bai, S. H. Chae, Q. Li, J. Wang, J. Hone, and X.-Y. Zhu, Science **367**, 903 (2020).
[99]O. Ambrozaite, R. Dziobek-Garrett, and T. J. Kempa, Acc. Chem. Res. **58**, 2216 (2025).
[100]S. Shree, I. Paradisanos, X. Marie, C. Robert, and B. Urbaszek, Nat. Rev. Phys. **3**, 39 (2021).
[101]H. Ardekani, R. Younts, Y. Yu, L. Cao, and K. Gundogdu, ACS Appl. Mater. Interfaces **11**, 38240 (2019).
[102]S. V. Sivaram, A. T. Hanbicki, M. R. Rosenberger, G. G. Jernigan, H.-J. Chuang, K. M. McCreary, and B. T. Jonker, ACS Appl. Mater. Interfaces **11**, 16147 (2019).

26 March 2026 13:26:42

© Author(s) 2026

[103]R. Rao, V. Carozo, Y. Wang, A. E. Islam, N. Perea-Lopez, K. Fujisawa, V. H. Crespi, M. Terrones, and B. Maruyama, 2D Mater. **6**, 045031 (2019).
[104]J. C. Kotsakidis, Q. Zhang, A. L. Vazquez de Parga, M. Currie, K. Helmerson, D. K. Gaskill, and M. S. Fuhrer, Nano Lett. **19**, 5205 (2019).
[105]J. M. Solomon, S. I. Ahmad, A. Dave, L.-S. Lu, Y.-C. Wu, W.-H. Chang, C.-W. Luo, and T.-H. Her, AIP Adv. **12**, 015217 (2022).
[106]J. M. Solomon, S. I. Ahmad, A. Dave, L.-S. Lu, F. HadavandMirzaee, S.-C. Lin, S.-H. Chen, C.-W. Luo, W.-H. Chang, and T.-H. Her, Sci. Rep. **12**, 6910 (2022).
[107]P. K. Poddar, Y. Zhong, A. J. Mannix, F. Mujid, J. Yu, C. Liang, J.-H. Kang, M. Lee, S. Xie, and J. Park, Nano Lett. **22**, 726 (2022).
[108]Z. Zhang, Z. Huang, J. Li, D. Wang, Y. Lin, X. Yang, H. Liu, S. Liu, Y. Wang, B. Li, X. Duan, and X. Duan, Nat. Nanotechnol. **17**, 493 (2022).
[109]Z. Huang, W. Deng, Z. Zhang, B. Zhao, H. Zhang, D. Wang, B. Li, M. Liu, Y. Huangfu, and X. Duan, Adv. Mater. **35**, 2211252 (2023).
[110]M. C. Lemme, D. Akinwande, C. Huyghebaert, and C. Stampfer, Nat. Commun. **13**, 1392 (2022).
[111]A. Thean, S.-H. Tsai, C.-K. Chen, M. Sivan, B. Tang, S. Hooda, Z. Fang, J. Pan, J. Leong, H. Veluri, and E. Zamburg, in *2022 International Electron Devices Meeting (IEDM)* (IEEE, 2022), pp. 12.2.1–12.2.4.
[112]C. Anichini, W. Czepa, D. Pakulski, A. Aliprandi, A. Ciesielski, and P. Samorí, Chem. Soc. Rev. **47**, 4860 (2018).
[113]J. van de Groep, J.-H. Song, U. Celano, Q. Li, P. G. Kik, and M. L. Brongersma, Nat. Photon. **14**, 426 (2020).
[114]L. Guarneri, Q. Li, T. Bauer, J.-H. Song, A. P. Saunders, F. Liu, M. L. Brongersma, and J. van de Groep, Nano Lett. **24**, 6240 (2024).
[115]S. R. Cho, S. Ahn, S. H. Lee, H. Ha, T. S. Kim, M.-K. Jo, C. Song, T. H. Im, P. Rani, M. Gyeon, K. Cho, S. Song, M. S. Jang, Y.-H. Cho, K. J. Lee, and K. Kang, Adv. Funct. Mater. **31**, 2105302 (2021).
[116]J. J. McMorrow, C. D. Cress, H. N. Arnold, V. K. Sangwan, D. Jariwala, S. W. Schmucker, T. J. Marks, and M. C. Hersam, Appl. Phys. Lett. **110**, 073102 (2017).
[117]V. Faramarzi, E. de Poortere, S. P. Venugopalan, P. Woltgens, Y. Woo, M. van de Kerkhof, P. Kumar, H. M. Silva, P. Morin, I. Asselberghs, C. Dorow, K. O'Brien, K. Maxey, and U. Avci, Proc. SPIE **12956**, 129560I (2024).
[118]M.-Y. Kao, C.-H. Hsu, Y.-Q. Huang, Y.-C. Hsu, M.-J. Liu, C.-T. Chen, P.-C. Lai, M.-Y. Lu, P.-J. Wu, and Y.-L. Chueh, ACS Appl. Electron. Mater. **6**, 5640 (2024).
[119]R. L. Brainard, G. G. Barclay, E. H. Anderson, and L. E. Ocola, Microelectron. Eng. **61-62**, 707 (2002).
[120]C. Luo, C. Xu, L. Lv, H. Li, X. Huang, and W. Liu, RSC Adv. **10**, 8385 (2020).
[121]A. Balena, M. Bianco, F. Pisanello, and M. De Vittorio, Adv. Funct. Mater. **33**, 2211773 (2023).
[122]C. Mauclair, B. Najih, V. Comte, F. Bourquard, and M. Delaigue, Opto-Electron. Sci. **4**, 250002 (2025).
[123]T. Pinheiro, M. Morais, S. Silvestre, E. Carlos, J. Coelho, H. V. Almeida, P. Barquinha, E. Fortunato, and R. Martins, Adv. Mater. **36**, 2402014 (2024).
[124]L. Cruciani, M. Vreugdenhil, D. van Oosten, K. van Druten, and P. Planken, Opt. Mater. Express **15**, 1005 (2025).
[125]W. Steinhögl, G. Schindler, G. Steinlesberger, M. Traving, and M. Engelhardt, J. Appl. Phys. **97**, 023706 (2005).
[126]D. Josell, S. H. Brongersma, and Z. Tőkei, Annu. Rev. Mater. Res. **39**, 231 (2009).
[127]D. Choi and K. Barmak, Electron. Mater. Lett. **13**, 449 (2017).
[128]T. M. Philip, N. A. Lanzillo, T. Gunst, T. Markussen, J. Cobb, S. Aboud, and R. R. Robison, Phys. Rev. Appl. **13**, 044045 (2020).
[129]E. Milosevic, S. Kerdsongpanya, A. Zangiabadi, K. Barmak, K. R. Coffey, and D. Gall, J. Appl. Phys. **124**, 165105 (2018).
[130]E. Abram, "Contours," version 1.0.0 (2024); see https://git.amolf.nl/Light-Matter_Interaction/contour.git.
[131]S. J. Byrnes, "Multilayer optical calculations," arXiv:1603.02720 (2020).
[132]N. A. Ukirade, Next Mater. **6**, 100479 (2025).

26 March 2026 13:26:42

© Author(s) 2026